

INFORMATION TO USERS

This material was produced from a microfilm copy of the original document. While the most advanced technological means to photograph and reproduce this document have been used, the quality is heavily dependent upon the quality of the original submitted.

The following explanation of techniques is provided to help you understand markings or patterns which may appear on this reproduction.

1. The sign or "target" for pages apparently lacking from the document photographed is "Missing Page(s)". If it was possible to obtain the missing page(s) or section, they are spliced into the film along with adjacent pages. This may have necessitated cutting thru an image and duplicating adjacent pages to insure you complete continuity.
2. When an image on the film is obliterated with a large round black mark, it is an indication that the photographer suspected that the copy may have moved during exposure and thus cause a blurred image. You will find a good image of the page in the adjacent frame.
3. When a map, drawing or chart, etc., was part of the material being photographed the photographer followed a definite method in "sectioning" the material. It is customary to begin photoing at the upper left hand corner of a large sheet and to continue photoing from left to right in equal sections with a small overlap. If necessary, sectioning is continued again – beginning below the first row and continuing on until complete.
4. The majority of users indicate that the textual content is of greatest value, however, a somewhat higher quality reproduction could be made from "photographs" if essential to the understanding of the dissertation. Silver prints of "photographs" may be ordered at additional charge by writing the Order Department, giving the catalog number, title, author and specific pages you wish reproduced.
5. PLEASE NOTE: Some pages may have indistinct print. Filmed as received.

University Microfilms International

300 North Zeeb Road
Ann Arbor, Michigan 48106 USA
St. John's Road, Tyler's Green
High Wycombe, Bucks, England HP10 8HR

7820429

LEE, SEUNG-MAN
A NUMERICAL STUDY OF THE EFFECT OF CLOUD
NUCLEI ON THE INITIATION OF RAIN FROM WARM
CLOUDS.

UNIVERSITY OF HAWAII, PH.D., 1978

A NUMERICAL STUDY
OF THE EFFECT OF CLOUD NUCLEI
ON THE INITIATION OF RAIN FROM WARM CLOUDS

A DISSERTATION SUBMITTED TO THE GRADUATE DIVISION OF THE
UNIVERSITY OF HAWAII IN PARTIAL FULFILLMENT
OF THE REQUIREMENTS FOR THE DEGREE OF

DOCTOR OF PHILOSOPHY

IN METEOROLOGY

MAY 1978

By

Seung-Man Lee

Dissertation Committee:

Tsutomu Takahashi, Chairman
Lajpat R. Ahuja
Charles M. Fullerton
Takio Murakami
Thomas A. Schroeder

ACKNOWLEDGMENTS

The author expresses his gratitude to Professor Tsutomu Takahashi, under whose sponsorship this research was carried out, for his guidance and encouragement. He also wishes to thank all the members of the Cloud Physics Observatory Staff who assisted in various ways. Computations were carried out on the CDC 7600 computer at the National Center for Atmospheric Research. The author wishes to thank Dr. R. Valent, of N.C.A.R., for his expert assistance.

ABSTRACT

The effects of the cloud nucleus size distribution and number concentration on rain initiation from shallow maritime warm clouds are examined in a one-dimensional, time-dependent cylindrical cloud model. Calculations include nucleation, condensation on both nuclei and drops, collection of drops and scavenging of nucleus-size particles to drops. It was found that nuclei of mass about 10^{-15} g are most efficient for warm rain development and the number concentration normally observed near Hawaii is the optimum concentration for maximum rainfall.

TABLE OF CONTENTS

	Page
ACKNOWLEDGMENTS	iii
ABSTRACT	iv
LIST OF ILLUSTRATIONS	vi
CHAPTER I. INTRODUCTION	1
CHAPTER II. FORMULATION OF MODEL	7
Physical processes included in the model	7
Basic equations	8
CHAPTER III. NUMERICAL PROCEDURE	17
Sequence of calculations	17
Size classification	18
Environmental and initial conditions	20
Condensation in the nucleus size range	20
Condensation-Collection in the drop size range	28
Dynamics	33
CHAPTER IV. RESULTS OF EXPERIMENTS	34
With normally observed nucleus size distribution	34
With different nucleus size ranges	38
With different nucleus concentrations	39
CHAPTER V. DISCUSSION AND CONCLUSIONS	41
APPENDIX LIST OF SYMBOLS	80
LITERATURE CITED	85

LIST OF ILLUSTRATIONS

Figure		Page
1.	Particle size and drop size classifications . .	49
2.	Flow diagram illustrating the sequence of calculations	50
3.	Dry salt particle concentration in terms of mass	51
4.	Environmental temperature and relative humidity profiles	52
5.	Redistribution of particles after 2 sec growth by condensation	53
6.	Time evolution of nucleus spectra through condensation process	54
7.	Time evolution of the drop mass density function through the condensation-collection process	55
8.	Time-height variation of vertical velocity and supersaturation for the case of the observed nucleus distribution	56
9.	Time-height variation of radial velocity for the case of the observed nucleus distribution .	57
10.	Time-height variation of temperature differences from environment for the case of the observed nucleus distribution	58
11.	Time-height variation of drop concentration for the case of the observed nucleus distribution	59
12.	Time-height variation of the liquid water mixing ratio for the case of the observed nucleus distribution	60
13.	Time-height variation of salt content for the case of the observed nucleus distribution .	61

Figure	Page
14. Time variation of the salt content of rainwater	62
15. Wet salt particle and drop density profiles at $t = 0$, with observed nucleus distribution .	63
16. Same as Fig. 15 except at $t = 10$ min	64
17. Same as Fig. 15 except at $t = 20$ min	65
18. Same as Fig. 15 except at $t = 30$ min	66
19. Same as Fig. 15 except at $t = 40$ min	67
20. Same as Fig. 15 except at $t = 50$ min	68
21. Same as Fig. 15 except at $t = 60$ min	69
22. Time-height variation of vertical velocity and supersaturation for the case of nucleus mass $< 10^{-15}$ g	70
23. Wet salt particle and drop density profiles at $t = 42$ min, with nucleus mass $< 10^{-15}$ g . .	71
24. Time-height variation of vertical velocity and supersaturation for the case of nucleus mass $< 10^{-17}$ g	72
25. Wet salt particle and drop density profiles at $t = 44$ min, with nucleus mass $< 10^{-17}$ g . .	73
26. Time-height variation of vertical velocity and supersaturation for the case of the standard nucleus concentration divided by ten	74
27. Wet salt particle and drop density profile at 42 min, with the standard nucleus concentration divided by ten	75
28. Time-height variation of vertical velocity and supersaturation for the case of the standard nucleus concentration multiplied by ten	76

Figure		Page
29.	Wet salt particle and drop density profiles at 56 min, with the standard nucleus concentration multiplied by ten	77
30.	Ratio of total rainfall amount with different nucleus size ranges to that for the case with the standard nucleus distribution	78
31.	Ratio of total rainfall amount with different nucleus concentrations to that for the case with the standard nucleus distribution	79

CHAPTER I
Introduction

In tropical regions, rain falls frequently from warm clouds. Cloud droplets form on nuclei of various sizes with activation determined by supersaturation. In early stages of cloud development, droplets grow primarily by condensation. After drops become large enough, they grow mainly by collection, leading to the formation of raindrops. Cloud stability, whether a given cloud can precipitate or not, is determined by the speed with which such critical size drops ($r = 20 \mu\text{m}$) form and begin the collection process. The evolution of drop growth is dependent on the nucleus size distribution.

Findeisen (1939) found that the formation of raindrops by condensation alone requires far more time than that observed in natural clouds. He showed that rain could form in pure-water clouds (warm clouds) by collection, but he rejected this idea because there were few warm rain observations at the time. He suggested that large drops collected only a fraction of the smaller droplets in their paths. Langmuir (1948) discussed the development of rain by a chain reaction process of raindrop multiplication. Large raindrops fracture into smaller drops which are carried vertically upward in the cloud by updrafts and

subsequently grow into raindrops. These raindrops fall, again break up into smaller drops, and repeat the process.

Meanwhile, evidence of warm rain began to accumulate, especially from aircraft operations in tropical areas. The occurrence and major properties of warm rain in Hawaii were established by two field studies of Hawaiian warm clouds: "Project Shower" in 1954, and the "Warm Rain Project" in 1965. Subsequent investigations attempted to explain warm rain development by considering either condensation or collection, but not both.

Howell (1949) was the first to compute the evolution of droplet growth by condensation from a given nucleus size distribution with a fixed updraft. Mordy (1959) extended Howell's calculations with a more realistic initial distribution of nuclei and further refinement in the droplet growth equation. Neiburger and Chien (1960) calculated the drop size distribution at various cloud heights by assuming an updraft profile. Mason and Emig (1961) developed a simple model of cumulus growth which provided a dynamical framework for computation of the growth of a population of cloud droplets, allowing mixing with the environment. Mason and Chien (1962), using this simple dynamical model, computed the growth of droplets by condensation on a spectrum of salt nuclei. They could not,

however, simulate the formation of large drops which are usually observed in warm clouds.

Studies of drop growth by collection were also carried out. Bowen (1950) and Ludlam (1951) showed that showers could be produced by collection assuming the initial existence of large drops near cloud base. These large drops were thought to result from condensational growth on giant nuclei (Woodcock, 1950, 1951). Analysis of the collection process was further refined by Telford (1955) who showed that drops grow much faster by stochastic collection than by continuous collection. The stochastic model was modified (Golovin, 1963; Scott, 1968) and used to study the development of large drops in a closed system (Twomey, 1966; Berry, 1967). Similar calculations were carried out by Warshaw (1967, 1968) assuming a fixed updraft in a vertical column.

Kovetz and Olund (1969) studied drop evolution in a numerical model which included both condensation and collection within a vertical column. Nelson (1971) studied the initial development of warm rain in isolated tropical cumulus clouds by considering stochastic coalescence in a bounded updraft. For an input cloud droplet spectra, observed values at cloud base were used.

Ogura and Takahashi (1973) were the first to include both condensation and collection in a physically realistic

one-dimensional, time-dependent cloud model. They assumed an instantaneous formation of cloud droplets on nuclei which were typically observed at cloud base. They studied the evolution of rain in convective showers using this model. Similar studies were carried out in two-dimensional models (Takahashi, 1973, 1975; Soong, 1974).

Silverman and Glass (1973) extended these calculations to cloud nuclei in a time-dependent cloud model. They calculated the droplet distribution at cloud base separately in a closed system and then used this distribution in their one-dimensional cloud model.

Arnason and Greenfield (1972), and Clark (1973) included cloud nuclei in a two-dimensional model. They assumed that droplets formed instantaneously on nuclei. In other words, particle sizes were determined by the equilibrium relation at the predicted supersaturation and not by the growth equation.

In 1971, Woodcock et al. questioned the effect of giant nuclei on warm rain initiation. They measured the iodine-chlorine ratio in cloud nuclei and in raindrops, and found that the mean value of the I/Cl ratio for raindrops was about 2×10^{-3} . This ratio corresponds to salt particles, ranging in mass from 10^{-12} to 10^{-14} g. The mean ratio among giant salt particles (10^{-8} to 10^{-12} g) was about 3×10^{-4} , approximately one order of magnitude

smaller than that in raindrops (see Fig. 1 for mass ranges of various nucleus sizes). This finding suggested that, while giant nuclei may not be essential for raindrop growth in warm clouds, sea-salt particles in the mass range of 10^{-12} to 10^{-14} g may play an important role in the process.

In order to examine the Woodcock et al. (1971) conclusion, Takahashi (1976a) used finer resolution in the nucleus range (31 classes) and a smaller time step (0.01 sec) to calculate rainfall development in a one-dimensional model. Nuclei grew by condensation and then were transferred to the drop size range. Drops were returned to the nucleus range by evaporation, as the humidity decreased. As cloud modeling reached this degree of sophistication, it became possible to use numerical models to study the effect of cloud nuclei. Takahashi showed that, while giant nuclei may not be required for warm rain initiation, they may be important for chemical balance during cloud development. Takahashi, however, limited the cloud nuclei studied to large nuclei (mass greater than 5.5×10^{-16} g) because of computational considerations. The condensation scheme which he used (Kovetz and Olund, 1969) had a broadening effect which made it impossible to extend calculations to smaller size nuclei. Takahashi, therefore, could not determine the

nucleus size range most important for initiation of rain in warm clouds using his cloud model.

In the present study a new condensation scheme was developed and the nucleus size range was extended to smaller sizes. The purpose of this study was to determine the cloud nucleus size range and number concentration most effective for warm rain development. The condensation-collection process in the drop size range was tested by comparison with an analytical solution under simplified conditions. Several computer simulations were obtained for different nucleus size ranges and number concentrations using typical trade-wind weather as environmental and initial conditions. The accumulated rainfall during cloud lifetime was calculated for each case.

CHAPTER II

Formulation of Model

1. Physical processes included in the model.

A one-dimensional, time-dependent, cylindrical model (Asai and Kasahara, 1967) was used as a dynamical frame. This simple model allows considerable emphasis to be placed on microphysical processes and permits finer resolution of both the nucleus and drop size representations. The environmental field outside the inner cylinder was assumed to be constant, thus ignoring the effect of compensating motion. Although a one-dimensional model cannot simulate horizontal variations of cloud properties, the average values within the cylinder are well simulated for shallow clouds (Takahashi, 1975).

All nuclei are assumed to exist as wet salt particles whose sizes are in equilibrium with the initial value of relative humidity. The droplet size distribution was found to be insensitive to the chemical composition of the soluble material in the nucleus (Fitzgerald, 1974). The nucleus concentration above 3 km was assumed to be one-tenth the concentration below 3 km.

The initial updraft impulse was given near the cloud base. The temperature, humidity and particle number are

functions of advection, lateral eddy exchange and dynamic entrainment. From the resulting humidity and temperature distribution, new supersaturation is calculated, particles are activated and grow. The latent heat released by condensation modifies the humidity, temperature and updraft; hence interaction between dynamics and micro-physics occurs.

As cloud droplets grow larger, the collection process becomes effective, resulting in even larger drops and eventually in raindrops. The wet salt particles are scavenged by drops through Brownian motion, diffusio-phoresis (particles suspended in a non uniform, isothermal gas, move in the direction of the diffusion flux of the heavier gas components), and thermophoresis (suspended particles move toward the lower temperature).

2. Basic Equations

(a) Equation for vertical velocity, w :

$$\frac{\partial w}{\partial t} = -w \frac{\partial w}{\partial z} - \frac{2\alpha_0 |w|}{a} w + \frac{2}{a} U (w - w_a) + g \frac{T_v - T_{ve}}{T_{ve}} - g Q_w, \quad (1)$$

where t is time, α_0 mixing coefficient ($\alpha_0^2 = 0.1$ is used for all variables), a the radius of the cylinder, U the radial velocity, g the acceleration due to gravity and T_v the virtual temperature. Subscripts e denote

environmental quantities and a , values at the perimeter of the cylinder. Q_w , the liquid water mixing ratio, is given by

$$Q_w = \frac{1}{\rho} \left(\sum_{I=1}^{I_{max}} f_I X_I + \sum_{L=1}^{L_{max}} F_L X_L \right), \quad (2)$$

where ρ is the air density and f_I and F_L are the number of wet salt particles and drops per unit volume in the mass class represented by the x_I and X_L , respectively.

The terms on the right hand side of Eq. (1) from left to right are vertical advection, the lateral eddy exchange, dynamic entrainment, the buoyancy force and the drag force due to drops. The radial velocity, U , is determined from the mass continuity equation,

$$\frac{2}{a} U + \frac{1}{\rho} \frac{\partial}{\partial z} (\rho w) = 0. \quad (3)$$

For any variable ϕ , the value at the perimeter of the cloud (ϕ_a) assumes either the in-cloud value (ϕ) or the environmental value (ϕ_e) depending on the sign of radial velocity:

$$\begin{aligned} \phi_a &= \phi_e & \text{if } U < 0, \\ \phi_a &= \phi & \text{if } U \geq 0. \end{aligned}$$

(b) The thermodynamic equation:

$$\begin{aligned} \frac{\partial T}{\partial t} = & -W \frac{\partial T}{\partial Z} - \Gamma_d W + \frac{2\alpha_o^2}{a} |W| (T_e - T) \\ & + \frac{2}{a} U(T - T_a) + \frac{L_v}{C_p} \frac{\delta Q_w}{\delta t}, \end{aligned} \quad (4)$$

where T is the temperature, Γ_d the dry adiabatic lapse rate, L_v the latent heat of condensation, C_p the specific heat of air at constant pressure and $\delta Q_w/\delta t$ the rate of change of liquid water mixing ratio due to condensation.

(c) Equation for water vapor:

$$\frac{\partial Q_v}{\partial t} = -W \frac{\partial Q_v}{\partial Z} + \frac{2\alpha_o^2}{a} |W| (Q_{ve} - Q_v) + \frac{2}{a} U (Q_v - Q_a) - \frac{\delta Q_w}{\delta t}, \quad (5)$$

where Q_v is water vapor mixing ratio.

(d) Equations for wet salt particles (I class) and drops (L class):

$$\begin{aligned} \frac{\partial f_I}{\partial t} = & -W \frac{\partial f_I}{\partial Z} + \frac{2\alpha_o^2}{a} |W| (f_{Ie} - f_I) + \frac{2}{a} U (f_I - f_{Ia}) \\ & + \frac{f_I}{P} W \frac{\partial P}{\partial Z} + \left(\frac{\delta f_I}{\delta t} \right)_N + \left(\frac{\delta f_I}{\delta t} \right)_{C.E.} - \left(\frac{\delta f_I}{\delta t} \right)_{BTD}, \end{aligned} \quad (6)$$

$$\begin{aligned} \frac{\partial F_L}{\partial t} = & -(w - v_L) \frac{\partial F_L}{\partial Z} + \frac{2\alpha_o^2}{a} |W| (F_{Le} - F_L) + \frac{2}{a} U (F_L - F_{La}) \\ & + \frac{F_L}{P} (w - v_L) \frac{\partial P}{\partial Z} + \left(\frac{\delta F_L}{\delta t} \right)_N + \left(\frac{\delta F_L}{\delta t} \right)_{C.E.} + \left(\frac{\delta F_L}{\delta t} \right)_{Coll}. \end{aligned} \quad (7)$$

Here V_L is the terminal velocity of a drop of size L , $\left(\frac{\delta f_I}{\delta t}\right)_N$ the rate of wet salt particle number change through drop evaporation, $\left(\frac{\delta F_L}{\delta t}\right)_N$ the rate of drop number change through nucleation from wet salt particles, $\left(\frac{\delta f_I}{\delta t}\right)_{C.E.}$ and $\left(\frac{\delta F_L}{\delta t}\right)_{C.E.}$ the rates of changes in wet salt particles and drop numbers through condensation and evaporation, $\left(\frac{\delta f_I}{\delta t}\right)_{BTD}$ the rate of wet salt particle number change due to Brownian motion, thermophoresis and diffusiophoresis, and $\left(\frac{\delta F_L}{\delta t}\right)_{COLL}$ the rate of drop number change due to the collection process.

The equation for condensation on wet salt particles is written as

$$\left(\frac{\delta f_I}{\delta t}\right)_{C.E.} = - \frac{\partial}{\partial X_I} \left(f_I \frac{dX_I}{dt} \right), \quad (8)$$

and the growth equation of particles of mass X_I , taken from Fukuta and Walter (1970), is

$$\frac{dX_I}{dt} = \frac{4\pi r_I (H-A) G_I}{\left(\frac{ALv^2 M_w}{KRT^2 f_{3\alpha}} + \frac{1}{D \rho_{\infty} f_{3\beta}} \right)}. \quad (9)$$

In Eq. (9), $A = 1 + \frac{B}{r_I} - \frac{C}{r_I^3}$, an approximate expression (Mason, 1971) for the relative humidity (H) in equilibrium at the surface of a drop of radius r_I , containing a salt (molecular weight $W = 58$) nucleus of mass m_I' , where

$$B = \frac{3.2 \times 10^{-5}}{T} \quad \text{and} \quad C = \frac{8.6 m'_x}{W} ,$$

$G_I = 1 + 0.23 \text{Re}_I^{\frac{1}{2}}$, the ventilation coefficient (Mason, 1971) with Re the Reynolds number. M_w is the molecular weight of water, K the thermal conductivity of air, R the universal gas constant, $P_{s\infty}$ the saturation vapor density at temperature T and D the diffusion constant of water vapor in air.

$$f_{3\alpha} = \frac{r_x}{r_x + C_\alpha} \quad \text{and} \quad f_{3\beta} = \frac{r_x}{r_x + C_\beta} \quad \text{are correction}$$

terms for the heat and vapor transfer at the drop surface, where $C_\alpha = 1.7 \times 10^{-5} \alpha^{-1}$, $C_\beta = 1.5 \times 10^{-5} \beta^{-1}$, $\alpha = 1$ and $\beta = 0.03$.

The term $\left(\frac{\delta f_I}{\delta t}\right)_{\text{BTD}}$ is the sum of three terms expressing the change in particle density due to Brownian motion, thermophoresis and diffusiophoresis.

(i) Brownian motion (Zebel, 1966; Davies, 1966)

$$\left(\frac{\delta f_I}{\delta t}\right)_B = f_I \sum_{L=1}^{L_{\text{max}}} 4\pi r_L^2 G_L F_L V_B , \quad (10)$$

where:

$$V_B = \frac{D_a}{r_L} \left(1 + 0.3 \text{Re}_L^{\frac{1}{2}} S_{ca}^{\frac{1}{3}}\right), \quad D_a = B_x k T ,$$

$$B_I = (1 + 0.864\zeta + 0.29\zeta e^{-1.25/\zeta}) (6\pi\eta r_I)^{-1},$$

$$\zeta = \frac{\lambda}{r_I}, \quad \text{and} \quad S_{ca} = \frac{\eta}{Da\rho}.$$

Here Da is the diffusion coefficient of the particles, B_I the mobility, k Boltzmann's constant, S_{ca} the Schmidt number, η dynamic viscosity, and λ the mean free path of the air molecules.

(ii) Thermophoresis (Waldmann and Schmitt, 1966; Slinn and Hales, 1971)

$$\left(\frac{\delta f_I}{\delta t}\right)_T = f_I \sum_{L=1}^{L_{max}} 4\pi r_L^2 G_L F_L V_T, \quad (11)$$

where:

$$V_T = 2.9 \times 10^7 \frac{f_t}{P} \left[\frac{1}{4\pi r_L^2} \left(\frac{dX_L}{dt} \right)_{c.e.} \right],$$

$$f_t = 0.4 (1 + 1.25\zeta + 0.42 e^{-0.87/\zeta}) (K + 2.5\zeta Ha)$$

$$\times [(1 + 3.7\zeta) (2K + 5\zeta Ha + Ha)]^{-1}. \quad (12)$$

Here, K and Ha are the thermal conductivity of air and salt, P the atmospheric pressure and $\left(\frac{dX_L}{dt}\right)_{c.e.}$ the rate of change of mass for drop of mass X_L due to condensation.

(iii) Diffusiophoresis (Waldmann and Schmitt, 1966)

$$\left(\frac{\delta f_I}{\delta t}\right)_D = f_I \sum_{L=1}^{L_{\max}} 4\pi r_L^2 G_L F_L V_D, \quad (13)$$

where $V_D = 2.86 \times 10^3 \frac{T}{P} \left[\frac{1}{4\pi r_L^2} \left(\frac{dX_L}{dt}\right)_{C.E.} \right]$.

All of the coefficients used are taken at temperature $T = 25^\circ\text{C}$ and pressure $P = 1000$ mb.

(iv) Equations for the salt content of wet salt particles and drops.

$$\begin{aligned} \frac{\partial m_I}{\partial t} = & -W \frac{\partial m_I}{\partial Z} + \frac{2\alpha_0^2}{a} |W| (m_{Ie} - m_I) + \frac{2}{a} U (m_I - m_{Ia}) \\ & + \frac{W m_I}{P} \frac{\partial P}{\partial Z} + \left(\frac{\delta m_I}{\delta t}\right)_N + \left(\frac{\delta m_I}{\delta t}\right)_{C.E.} - \left(\frac{\delta m_I}{\delta t}\right)_{BTD}, \end{aligned} \quad (14)$$

$$\begin{aligned} \frac{\partial M_L}{\partial t} = & -(W - V_L) \frac{\partial M_L}{\partial Z} + \frac{2\alpha_0^2}{a} |W| (M_{Le} - M_L) + \frac{2}{a} U (M_L - M_{La}) \\ & + (W - V_L) \frac{M_L}{P} \frac{\partial P}{\partial Z} + \left(\frac{\delta M_L}{\delta t}\right)_N + \left(\frac{\delta M_L}{\delta t}\right)_{C.E.} + \left(\frac{\delta M_L}{\delta t}\right)_{COLL} + \left(\frac{\delta M_L}{\delta t}\right)_{BTD}. \end{aligned} \quad (15)$$

Here m_I and M_L are the salt content of wet salt particles of size (I) and drops of size (L), respectively. Other notations are the same as those used in the case of number density.

(v) Equation for the collection process

The equation follows from Berry (1967),

$$\begin{aligned} \left(\frac{\partial F_L}{\partial t}\right)_{\text{coll}} &= \int_1^{L_\alpha} \left(\frac{X_L}{X_{Lc}}\right) F_{Lc} V(Lc|L') F_{L'} dL' \\ &\quad - \int_1^\infty F_L V(L|L') F_{L'} dL' \end{aligned} \quad (16)$$

where:

$$L_\alpha = L - (DJ/3) \ln 2, \quad (17)$$

$$Lc = L + (DJ/3) \ln \{1 - \exp [3(L' - L)/DJ]\}, \quad (18)$$

$$V(L|L') = \pi Y_c^2 Y_c(L|L')^2 |v_L - v_{L'}|,$$

$$X_{Lc} = X_L - X_{L'},$$

$$r_L = r_0 \exp\left(\frac{L-1}{DJ}\right),$$

$$X_L = \left(\frac{4}{3} \pi r_0^3\right) \exp\left[\frac{3(L-1)}{DJ}\right].$$

Here r_L is the radius of drops of size (L) , $Y_c(L|L')$ the collision efficiency, r_0 the radius of the smallest drop ($1 \mu\text{m}$) and DJ the scale factor (8.658).

For collision efficiencies, Almeida's (1976) values are used for drops smaller than $60 \mu\text{m}$ in radius and those of Shafrir and Neiburger (1963) for drops larger than $60 \mu\text{m}$. Coalescence efficiency is assumed to be 1.

The terminal velocity is given by Stoke's law for

drops smaller than 40 μm in radius and by Gunn-Kinzer's values (1949) for larger drops:

$$V_L = 1.26 \times 10^6 \times r_L^2 \quad r_L < 40 \mu\text{m},$$

$$V_L = 8000 \times r_L \quad 40 \mu\text{m} < r_L < 500 \mu\text{m},$$

$$V_L = 1400 \times (2r_L)^{\frac{1}{2}} \quad 500 \mu\text{m} < r_L.$$

CHAPTER III
Numerical Procedure

1. Sequence of calculations (Fig. 2).

(a) After initialization advective changes in temperature and the water vapor mixing ratio are calculated in a 2 sec time step (upstream scheme). The new supersaturation is calculated.

(b) Using the new supersaturation, condensation on wet salt particles is calculated using the new scheme. The temperature is adjusted by including latent heat release. The water vapor mixing ratio is modified by subtracting the amount of condensate.

(c) New wet salt concentrations, drop concentrations and vertical velocity are calculated in a time step of 2 sec. The radial velocity is determined from continuity.

(d) A new supersaturation is calculated, based on the adjusted temperature and water vapor mixing ratio from step (b) above. Condensation in the drop size range is calculated in a 2 sec time step. The temperature and water vapor mixing ratio again are adjusted.

(e) Steps (a) and (d) are repeated ten times.

(f) Collection and scavenging then are calculated in

a 20 sec time step.

This completes one cycle of calculation, advancing 20 sec in time (forward scheme).

2. Size classifications.

(a) Dry salt size classes are defined by:

$$r_k = r_0 \exp [(k-1)/DJ], \quad (19)$$

where r_0 is the radius of the smallest particle (0.007 μm), DJ a scale factor (8.658) and k an integer ranging from 1 to 64. The size range is 0.007 to 10 μm in radius with mass corresponding to the dry salt particle radii shown in Fig. 1.

The distribution of dry salt particles of mass less than 3.3×10^{-16} g is taken from Jiusto (1967). The total number of particles activated, $N(\text{cm}^{-3})$, at supersaturation σ is expressed as,

$$N = 53 (\sigma \times 100)^{0.46}, \quad (20)$$

The critical supersaturation σ_c for a salt mass (m) is given by,

$$\sigma_c = \left(\frac{4B^3}{27C} \right)^{\frac{1}{2}}, \quad (21)$$

where $B = 1.1 \times 10^{-7}$ and $C = \frac{8.6}{W} m$. Particles of mass m grow if supersaturation σ exceeds σ_c . The particle concentration of mass greater than m is given in the following form, combining Eqs. (20) and (21),

$$N = 53 \left[\left(\frac{B^3}{m} \right)^{\frac{1}{2}} \times 100 \right]^{0.46}$$

The distribution for larger particles (Fig. 3) is obtained from Woodcock (1972).

(b) Wet salt particles--The size range consists of 44 classes defined by a relation similar to Eq. (19). In this case k is replaced by I , which ranges from 1 to 44. The size range is 0.007 to 1 μm in radius. Dry salt particles absorb water vapor and transform into wet salt particles according to the initial relative humidity profile. The salt mass m'_I , contained in a wet salt particle of radius r_I in equilibrium with the environmental relative humidity, is calculated from the following relationship:

$$m'_I = \frac{58}{8.6} [B r_I^2 - r_I^3 (H-1)].$$

(c) Drops--The drops are divided into 71 classes by a relation similar to Eq. (19). The range of radii is 1 to

3250 μm , r_0 is 1 μm and k is replaced by L , which ranges from 1 to 71.

3. Environmental and initial conditions.

The upper air temperature and relative humidity values (Fig. 4) observed on 23 May 1971 in Hilo, Hawaii, are assumed as typical of trade-wind conditions. The temperature inversion appears at 3 km, while the humidity discontinuity occurs at 2 km. Although these conditions differ somewhat from the conventional view of trade-wind soundings (Riehl, 1954), the stable layer (lapse rate 3 $^{\circ}\text{C km}^{-1}$) extends upward from the 2 km level. Workers in Hawaii are familiar with soundings of this type.

The initial updraft is given by:

$$W = \Delta W \sin^2\left(\frac{\pi Z}{2z_0}\right),$$

in the layer below 2 km, where $\Delta w = 1 \text{ m sec}^{-1}$ and $z_0 = 1 \text{ km}$. The vertical velocity and drops vanish both at the surface and at the top of the atmosphere (assumed to be at 4 km), and other values are fixed at these boundaries. The radius of the cloud is assumed to be 1 km.

4. Condensation in the nucleus size range.

A new scheme was developed for calculating condensation in the nucleus size range. To represent the

wet salt particle distribution, a radius class (K) containing f_K particles is defined at each edge of radii, $RO(K)$ and $RO(K+1)$ (Fig. 5). The mean salt content is calculated at $RO(K+\frac{1}{2})$ by dividing the total salt content by f_K . The mean salt content at $RO(K)$ then is determined by interpolation of the values at $RO(K-\frac{1}{2})$ and $RO(K+\frac{1}{2})$ with respect to particle volume.

The growth equation (9) is numerically integrated at $RO(K)$ for 2 sec. At each time step, the first-order stability condition for condensation is checked and the succeeding time step modified according to the following conditions:

- i) if $\left| \frac{1}{r_x} \frac{dr_x}{dt} \Delta t \right|_{\max} \geq 1$, the time step is reduced to $\frac{\Delta t}{10}$;
- ii) if $0.1 < \left| \frac{1}{r_x} \frac{dr_x}{dt} \Delta t \right|_{\max} < 1$, the time step is not changed;
- iii) if $\left| \frac{1}{r_x} \frac{dr_x}{dt} \Delta t \right|_{\max} < 0.1$, the time step is increased to $10\Delta t$.

The initial time step was taken as 10^{-5} sec and increased to 0.1 sec. A particle grows from $RO(K)$ to $RT(K)$ in 2 sec.

The particles f_K in class K [$RO(K), RO(K+1)$] are distributed over a new size range [$RT(K), RT(K+1)$] after 2 sec growth (Fig. 5). The contribution of f_K between $RO(I)$ and $RO(I+1)$, f_{IK}^* , is given by,

$$f_{IK}^* = f_K \frac{[RO(I+1) - RT(K)]}{[RT(K+1) - RT(K)]} \quad (22)$$

The particle concentration, f_I^* , between RO(I) and RO(I+1) is summed and defined as the concentration of the I'th class. Salt content is obtained in the same manner. The scheme conserves both the total nucleus number and salt content.

The new calculation scheme was compared with an analytic solution in a simplified case.

The growth equation (9) was simplified by assuming

$$f_{3\alpha} = f_{3\beta} = 1 \quad \text{and}$$

$$\frac{L_v^2 M_w}{KRT^2 f_{3\alpha}} + \frac{1}{D P_{s\infty} f_{3\beta}} = D_f = \text{Constant}. \quad (23)$$

The equation can be rearranged into the form,

$$\frac{dr}{dt} = \frac{1}{D_f} \left(\frac{\sigma}{r} - \frac{B}{r^2} + \frac{C}{r^4} \right), \quad (24)$$

where σ is supersaturation and r the radius. The time required for the particle to grow from radius r_c to r_t is obtained by integration of Eq. (24),

$$t = \frac{D_f}{\sigma} \left[\int_{r_0}^{r_t} (r - a') dr + \int_{r_0}^{r_t} \frac{a'^2 r^2 - c' r + a' c'}{r^3 + a' r^2 + c'} dr \right], \quad (25)$$

where $a' = -\frac{B}{\sigma}$ and $c' = \frac{C}{\sigma}$.

To integrate the second term of the right hand side

of Eq. (25), the roots of the following cubic equation were sought:

$$r^3 + a'r^2 + c' = 0. \quad (26)$$

Using Cardan's method (Korn and Korn, 1961) Eq. (26) is transformed by defining $r \equiv y - \frac{a'}{3}$,

$$y^3 + py + q = (y-Y_1)(y-Y_2)(y-Y_3) = 0. \quad (27)$$

The transitional coefficients p and q , and the three roots Y_1 , Y_2 , and Y_3 are expressed as

$$p = -\frac{a'^2}{3}, \quad q = 2\left(\frac{a'}{3}\right)^3 + c',$$

$$Y_1 = A' + B',$$

$$Y_2 = -\frac{A' + B'}{2} + i \frac{A' - B'}{2} \sqrt{3},$$

$$Y_3 = -\frac{A' + B'}{2} - i \frac{A' - B'}{2} \sqrt{3},$$

where:

$$Q = \left(\frac{p}{3}\right)^3 + \left(\frac{q}{2}\right)^2, \quad (28)$$

$$A' = \left(-\frac{q}{2} + \sqrt{Q}\right)^{\frac{1}{3}}, \quad (29)$$

$$B' = \left(-\frac{q}{2} - \sqrt{Q}\right)^{\frac{1}{3}}. \quad (30)$$

Depending on the value of Q , Eq. (25) has three different solutions.

i) If $Q > 0$,

$$t = \frac{D_f}{\sigma} \left\{ \left(\frac{r^2}{2} - a'r \right) + E \ln(r + A_1) + \frac{F}{2} \ln(r^2 + A_2 r + A_3) \right. \\ \left. + \frac{(G - \frac{F}{2} A_2)}{\sqrt{A_3 - \frac{A_2^2}{4}}} \left[\tan^{-1} \left(\frac{r + \frac{A_2}{2}}{\sqrt{A_3 - \frac{A_2^2}{4}}} \right) \right] \right\}_{r_0}^{r_t}, \quad (31)$$

where:

$$A_1 = \frac{a'}{3} - y_1,$$

$$A_2 = \frac{a'}{3} - (y_2 + y_3),$$

$$A_3 = \left(\frac{a'}{3} \right)^2 - (y_2 + y_3) \frac{a'}{3} + y_2 y_3,$$

$$E = (a'^2 A_1^2 + a'c' + c'A_1) / \Delta,$$

$$F = (a'^2 A_3 - c'A_1 - a'c' - a'^2 A_2 A_1) / \Delta,$$

$$G = (a'c'A_1 - c'A_3 - a'c'A_2 - a'^2 A_1 A_3) / \Delta,$$

$$\Delta = A_1^2 + A_3 - A_1 A_2.$$

ii) If $Q = 0$,

$$t = \frac{D_f}{\sigma} \left[\left(\frac{r^2}{2} - a'r \right) + E' \ln(r + A'_1) + G' \ln(r + A'_2) - \left(\frac{F'}{r + A'_2} \right) \right]_{r_0}^{r_t}, \quad (32)$$

where:

$$A'_1 = \frac{a'}{3} - 2 \left(-\frac{q'}{2} \right)^{\frac{1}{3}},$$

$$A'_2 = \frac{a'}{3} + \left(-\frac{q'}{2} \right)^{\frac{1}{3}},$$

$$E' = (-c'A'_1 - a'^2 A_1'^2 - a'c') / \Delta',$$

$$F' = (-c'A'_1 A'_2 - a'^2 A_1' A_2'^2 + a'^2 A_2'^2 - a'c'A'_1 + a'c'A'_2 + c'A_2'^2) / \Delta',$$

$$G' = (a'c' + 2a'^2 A_1' A_2' + c'A'_1 - a'^2 A_2'^2) / \Delta',$$

$$\Delta' = 2A_1' A_2' - A_1'^2 - A_2'^2.$$

iii) If $Q < 0$,

$$t = \frac{D_f}{\sigma} \left[\left(\frac{r^2}{2} - a'r \right) + E'' \ln(r + A''_1) + F'' \ln(r + A''_2) + G'' \ln(r + A''_3) \right]_{r_0}^{r_t}, \quad (33)$$

where:

$$A_1'' = \frac{a'}{3} - y_1, \quad A_2'' = \frac{a'}{3} - y_2, \quad A_3'' = \frac{a'}{3} - y_3,$$

$$y_1 = 2\sqrt{-P/3} \cos(\delta/3),$$

$$y_2 = -2\sqrt{-P/3} \cos(\delta/3 + \pi/3),$$

$$y_3 = -2\sqrt{-P/3} \cos(\delta/3 - \pi/3),$$

$$\left. \begin{aligned} \delta &= \tan^{-1} [\sqrt{-Q} / (-P/2)] , & \text{if } P \leq 0 \\ \delta &= \tan^{-1} [\sqrt{-Q} / (-P/2)] + \pi & \text{if } P > 0 \end{aligned} \right\} \quad (34)$$

$$\Delta'' E'' = \begin{vmatrix} a'^2 & 1 & 1 \\ -c' & A_1'' + A_3'' & A_1'' + A_2'' \\ a'c' & A_1'' A_3'' & A_1'' A_2'' \end{vmatrix},$$

$$\Delta'' F'' = \begin{vmatrix} 1 & a'^2 & 1 \\ A_2'' + A_3'' & -c' & A_1'' + A_2'' \\ A_2'' A_3'' & a'c' & A_1'' A_2'' \end{vmatrix},$$

$$\Delta'' G = \begin{vmatrix} 1 & 1 & a'^2 \\ A_2'' + A_3'' & A_1'' + A_3'' & -c' \\ A_2'' A_3'' & A_1'' A_3'' & a'c' \end{vmatrix},$$

$$\Delta'' = \begin{vmatrix} 1 & 1 & 1 \\ A_2'' + A_3'' & A_1'' + A_3'' & A_1'' + A_2'' \\ A_2'' A_3'' & A_1'' A_3'' & A_1'' A_2'' \end{vmatrix}.$$

The time (t_{IK}) required for a nucleus of radius r_I to grow to r_K , is calculated. Nucleus size after 2 sec growth is determined by interpolation with respect to t_{IK} .

The time evolutions of nucleus spectra computed by the new calculation scheme, the Kovetz-Olund (1969) method and the analytical solution were compared (Fig. 6). The initial nucleus distribution is derived from Woodcock (1972) and is assumed to be in equilibrium at 90% relative humidity. Supersaturation is fixed at 0.1% and the temperature at 17°C. Nucleus sizes are defined in the form given by Eq. (19), with $r_0 = 0.0312 \mu\text{m}$. The spectrum computed by the present scheme is close to that derived by

the analytical solution. The Kovetz-Olund scheme produced an oscillation for radii less than 0.7 μm but matches the analytical solution closely for particles larger than 0.8 μm .

5. Condensation-Collection in the drop size range.

The Kovetz-Olund method was used to calculate drop condensation. Berry's scheme (1967) was used to calculate collection. The combined schemes were compared with an approximate analytical solution.

By assuming a constant condensation rate (c_0) and constant collision kernel (b), the rate of change in drop concentration may be expressed in a coordinate system moving with speed c_0 , as

$$\frac{\partial}{\partial t} f(v,t) = \frac{b}{2} \int_0^v f(u,t) f(v-u-c_0t,t) du - b \int_0^\infty f(u,t) f(v,t) du, \quad (35)$$

where $f(v,t)$ is the concentration at drop mass v and time t , and u the mass of a drop colliding with a drop of mass v . The solution is obtained in a manner similar to that of Golovin (1963) who solved for collision only.

An exponential function of mass was chosen as the initial drop size distribution:

$$f(v,0) = \frac{N_0}{v_0} \exp\left(-\frac{v}{v_0}\right). \quad (36)$$

The concentration $f(v,t)$ is rewritten in the form

$$f(v,t) = \frac{N_0}{v_0} \psi(x, \tau), \quad (37)$$

where $x \equiv v/v_0$ and τ is the fraction of N_0 removed by collection at time t . The total number of drops at t is written as follows,

$$\int_0^{\infty} f(v,t) dv = N_0 (1 - \tau). \quad (38)$$

From Eqs. (37) and (38), it follows that

$$\int_0^{\infty} \psi(x, \tau) dx = 1 - \tau. \quad (39)$$

The rate of change in total drop concentration at time t due to collection is written as,

$$\frac{d}{dt} \left[\int_0^{\infty} f(v,t) dv \right] = -\frac{b}{2} \int_0^{\infty} \int_0^{\infty} f(v,t) f(u,t) du dv. \quad (40)$$

From Eqs. (38) and (40), it follows that

$$\frac{d\tau}{dt} = \frac{b}{2} N_0 (1 - \tau)^2. \quad (41)$$

Integration of Eq. (41) yields,

$$1 - \tau = \frac{1}{1 + \frac{bN_0 t}{2}}. \quad (42)$$

Using Eqs. (37), (38), and (41), Eq. (35) can be expressed in terms of $\psi(x, \tau)$,

$$(1-\tau)^2 \frac{\partial}{\partial \tau} \psi(x, \tau) = \int_0^x \psi(y', \tau) \psi(x-y' - \frac{c_0}{v_0} t, \tau) dy' - 2\psi(x, \tau)(1-\tau). \quad (43)$$

For small values of $\frac{c_0}{v_0} t (< 1)$, $\psi(x-y' - \frac{c_0}{v_0} t, \tau)$ may be approximated by taking the first-order term of the Taylor expansion,

$$\psi(x-y' - \frac{c_0}{v_0} t, \tau) \approx \psi(x-y', \tau) - \frac{c_0}{v_0} t \frac{\partial}{\partial (x-y')} \psi(x-y', \tau).$$

Substituting $\xi = x - y'$, Eq. (43) is written as,

$$(1-\tau)^2 \frac{\partial}{\partial \tau} \psi(x, \tau) = \int_0^x \psi(y', \tau) \psi(x-y', \tau) dy' - \frac{c_0}{v_0} t \int_0^x \psi(x-\xi, \tau) \frac{\partial}{\partial \xi} \psi(\xi, \tau) d\xi - 2\psi(x, \tau)(1-\tau) \quad (44)$$

Using the following Laplace transformation,

$$\int_0^{\infty} e^{-sx} \psi(x, \tau) dx = (1-\tau) \Phi(s, \tau), \quad (45)$$

Eq. (44) is transformed into the expression:

$$(1-\tau)^2 \frac{\partial}{\partial \tau} \Phi(s, \tau) + \Phi(s, \tau) = \left(1 - \frac{sA_0\tau}{1-\tau}\right) \Phi(s, \tau)^2, \quad (46)$$

where $A_0 = \frac{2c_0}{N_0 v_0 b}$

From the characteristic equation of Eq. (46) it follows that

$$S = C_1 .$$

For a given value of S , $\Phi(S, \tau)$ is a function of τ only and the differential equation may be written as,

$$\frac{d}{d\tau} \Phi(s, \tau) + \frac{1}{1-\tau} \Phi(s, \tau) = \left(\frac{1}{1-\tau} - \frac{sA_0\tau}{(1-\tau)^2} \right) \Phi(s, \tau) \quad (47)$$

The solution of Eq. (47) is given by

$$\frac{1}{\Phi(s, \tau)} (1-\tau) = -\tau + sA_0[-\tau - \ln(1-\tau)] + C_2 \quad (48)$$

The constant of integration C_2 is determined by the relation,

$$\int_0^{\infty} e^{-sx} \psi(x, 0) dx = \frac{1}{1+s} = \Phi(s, 0),$$

and from Eq. (48), with $\tau = 0$, it follows that

$$\frac{1}{\Phi(s, 0)} = C_2.$$

Then Eq. (48) may be arranged in the form,

$$\Phi(s, \tau) = \frac{\left\{ \frac{1-\tau}{1-A_0[\tau + \ln(1-\tau)]} \right\}}{s + \left\{ \frac{1-\tau}{1-A_0[\tau + \ln(1-\tau)]} \right\}} \quad (49)$$

An inverse Laplace transform of Eq. (49) will give the solution,

$$\Psi(x, \tau) = \frac{(1-\tau)^2}{H_0} \exp\left[-\frac{(1-\tau)x}{H_0}\right], \quad (50)$$

where $H_0 \equiv 1 - A_0 [\tau + \ln(1-\tau)]$. (51)

In a fixed coordinate system, the final solution is written as

$$f(v, t) = \left(\frac{N_0}{v_0}\right) \frac{\exp[-(v - c_0 t)/(v_0 G_0)]}{G_0 D_0}, \quad (52)$$

where:

$$D_0 = 1 + \frac{b}{2} N_0 t, \quad (53)$$

$$G_0 = D_0 \left(1 - \frac{c_0 t}{v_0 D_0} + \frac{2c_0}{N_0 v_0 b} \ln D_0\right). \quad (54)$$

The drop mass density is defined as,

$$g[\ln r(t)] = 3v^2 f(v, t).$$

The time evolution of drop mass density, $g(\ln r)$, was computed both by the numerical scheme and by the analytical solution for a case using the following values:

$$\begin{aligned} N_0 &= 50 \text{ cm}^{-3}, \\ v_0 &= 2.0 \times 10^{-8} \text{ g}, \\ c_0 &= 10^{-11} \text{ g sec}^{-1} \end{aligned}$$

and $b = 1.8 \times 10^{-4} \text{ cm}^3 \text{ sec}^{-1}$.

The result (Fig. 7) shows that the drop mass densities computed by the numerical method compare well with those computed by an analytical solution, at least under the simplified conditions specified.

6. Dynamics

A forward-upstream scheme is used with a vertical grid size of 200 m and a time step of 2 sec. Saturation vapor pressure is calculated by Tetten's formula (Asai and Kasahara, 1967). In-cloud supersaturation is modified after Asai (1965) who considered the change in supersaturation due to the temperature increase during condensation.

CHAPTER IV

Results of Experiments

1. With normally observed nucleus distribution.

(a) Vertical velocity, supersaturation and rainfall intensity.

Various results of the computer simulation will now be described, using a series of height versus time plots.

After the initial impulse, the updraft increased from 8 min above 0.8 km due to latent heat release by condensation (Fig. 8). The updraft speed increased with time reaching a maximum value of 3.1 m sec^{-1} at 26 min at 1.6 km. A small gravitational oscillation appeared above the cloud top. Following the formation of drizzle and raindrops in the upper portion of the cloud, the updraft decreased due to the drag force imparted by the drops. At around 40 min a downdraft originated near the ground.

An intense radial outflow occurred near cloud top, with a weak inflow below the cloud base (Fig. 9). Simultaneously with the development of the downdraft, outflow developed near the ground.

Near the cloud base, supersaturation remained almost constant at 0.8% (Fig. 8). At 30 min., supersaturation increased in the cloud because of the decrease in drop concentration due to collection. The decrease in drop concentration took place where cloud droplets were

converted rapidly to drizzle and raindrops (explained later in more detail). The maximum supersaturation (1.3%) occurred at 38 min at 2 km.

Rainfall began at 38 min and attained maximum intensity (23 mm h^{-1}) at 44 min (Fig. 8). A secondary peak in rainfall intensity occurred at 52 min, coincident with the development of the downdraft. The total rainfall during the cloud lifetime was 4.4 mm.

Near the cloud base and at 1.5 km, the in-cloud temperature was 0.2°C higher than the environment due to condensational heating. Strong evaporational cooling occurred near cloud top (Fig. 10).

(b) Drop concentration and liquid water content.

Drop concentration was a maximum (47 cm^{-3}) near the cloud base (Fig. 11). The value remained almost constant to about 40 min. The concentration decreased with height and decreased sharply after about 30 min in the upper portion of the cloud. This decrease in drop concentration is consistent with efficient drop growth by collection.

High liquid water contents occurred in the upper portion of the cloud (Fig. 12). A maximum cloud water content (1.0 g kg^{-1}) occurred at 24 min near 1.6 km. A maximum value of 1.3 g kg^{-1} for drizzle occurred near 1.8 km. There are two maxima for raindrops: 1.4 g kg^{-1} at

around 40 min and a secondary value of 0.57 g kg^{-1} near 50 min at a height of 1.2 km. These maxima caused two peak rainfall intensities.

(c) Salt content.

In all cases the minimum salt content occurred in the upper portion of the cloud (Fig. 13).

The minimum value of 3.3 mg l^{-1} occurred at 40 min near 2.2 km. The low value of salt content at cloud top followed the rainfall to the ground. The minimum salt content at the ground coincided with the second peak in rainfall intensity. The minimum rainwater salt content occurred again near the second peak (Fig. 14).

(d) Evolution of wet salt particle and drop density profiles.

The initial (at time 0) profiles of wet salt particle density, drop density and salt content are shown in Fig. 15.

At 10 min (Fig. 16), the nucleation of particles and condensation on drops occurred actively near the 1 km level. Above the cloud, complicated patterns appeared due to the oscillation of vertical velocity.

At 20 min (Fig. 17), the cloud grew to a height of 1.6 km. Small drizzle already formed between 1 and 1.4 km.

At 30 min (Fig. 18), the cloud developed further, reaching 2 km. In upper portion of the cloud, particles of mass less than 10^{-17} g were activated. Drops larger than 400 μ m in radius began to form in the upper portion of the cloud.

At 40 min (Fig. 19), particles of mass less than 10^{-17} g were activated in the layer between 1 and 2 km, as the cloud top reached 2.4 km. Raindrops larger than 1 mm in radius were produced.

At 50 min (Fig. 20), no further cloud development occurred. Near the ground cloud droplets of about 10 μ m radius were largely removed by evaporation.

At 60 min (Fig. 21), many small particles were resupplied by evaporation from drops as the cloud dissipated.

The salt content of a drop during condensation should not change and lines of equal salt content should parallel lines of equal drop density during condensational growth. Salt content increased during condensation, however. This result appears to be fictitious, arising from the numerical scheme employed. All particles are summed in each class irrespective of their history and only average salt mass in the class is recorded. The final results, however, are not significantly affected by this effect as shown in the later section.

2. With different nucleus size distribution.

The development of warm clouds and rainfall generally was well simulated by the cloud model used in this study (comparison with observations will be given in the discussion). Using this model, several experiments were carried out by specifying different nucleus size distributions and concentrations. The results will be described using illustrations similar to those used in the preceding section.

(a) Nuclei of mass greater than 10^{-15} g removed.

When nuclei of mass greater than 10^{-15} g were removed, the computed vertical velocity and total rainfall amount were almost the same as in the case of the standard nucleus distribution (nuclei distribution normally observed). The supersaturation is slightly higher and peak rainfall intensity slightly lower than the standard case (Fig. 22). The rainfall intensity decreased slowly from its peak value. The formation of drops larger than 20 μm in radius was delayed and the salt content was much lower than in the case using all nuclei (Fig. 23).

(b) Nuclei of mass greater than 10^{-17} g removed.

When nuclei of mass greater than 10^{-17} g were removed, the cloud was poorly developed (Fig. 24). Since nuclei were

small and particle growth slow (Fig. 25), the consumption of available moisture during condensation was small. This caused supersaturations as high as 2%. Due to reduced condensational heating, the updraft was weak and the cloud shallow. Raindrop size was small, rainfall intensity low and the total rainfall sharply reduced.

3. With different nucleus concentrations.

(a) Standard nucleus concentration divided by ten.

When the total nucleus concentration was decreased by one order of magnitude, the cloud was poorly developed due to reduced latent heating. The supersaturation rose as high as 3% (Fig. 26). Small particles, mass less than 10^{-17} g, were activated (Fig. 27) but the total droplet number was very small. Thus, the amount of condensed water was small, and a weakened updraft developed due to the small amount of latent heat released. The cloud was shallow, the raindrops small, the rainfall intensity weak and the total rainfall reduced.

(b) Standard nucleus concentration multiplied by ten.

When total nucleus concentration was increased by a factor of ten, the cloud developed to great height (2.6 km), but the onset of rain was delayed and the total rainfall amount was reduced (Fig. 28). Because of the large number of drops formed, there was considerable competition for

the available moisture and the maximum supersaturation was only 0.3%. Large amounts of latent heat were released because of the great volume of water condensed on numerous droplets. The updraft was well developed, reaching a maximum value of 3.6 m sec^{-1} . The conversion from cloud droplets to raindrops was slow, due to the small number of effective large droplets necessary to initiate the collection process (Fig. 29). However, the few raindrops formed were large, due to the strong updraft and the greater cloud depth. The cloud survived longer.

CHAPTER V

Discussion and Conclusions

1. Comparison with observations.

Results obtained using the present cloud model may be compared with observations made mainly near the island of Hawaii. Squires (1958) observed that rainfall began about half an hour after development of a 2 km deep cloud. Takahashi (1977) reported that rain starts falling from the base of an isolated warm cloud within 15 to 25 min and lasts about 20 min. The present cloud model indicates that rainfall commences at 38 min and continues for 28 min.

Differences between observations and numerical results may be due to assumptions inherent in the model. The environment outside of the cylindrical cloud is assumed to remain unchanged and compensating downward motion is not considered. A continuous supply of unmodified air and the lack of a damping effect due to compensating motion may combine to prolong cloud development. As a result, the onset of rainfall may be delayed and the shower may last longer in the model than in nature.

The calculated maximum rainfall intensity (23 mm hr^{-1}) is somewhat weaker than that observed by Takahashi (1976b). The weaker rainfall rate in the model may be due to averaging rainfall intensities over the cross section of

the cylinder.

The vertical velocity computed by the present model may be compared with observed values reported by Warner (1970). Although the observation was made near the coastline of eastern Australia, cloud dimensions were similar. Warner exhibited vertical velocity in the form of a root-mean-square updraft as a function of height. The maximum vertical velocity (2.83 m sec^{-1}) was observed between the 1.5 and 1.8 km levels. In the present model, it was 3.1 m sec^{-1} at 1.6 km. These values are remarkably similar even though the clouds have somewhat different properties resulting from local environmental conditions.

Present model results of supersaturation values near cloud base (0.4 to 0.8%) may be compared with values calculated (0.2 to 0.8%) by Twomey (1959) from observed cloud droplet and nucleus distributions for given updraft speeds.

The decrease in drop concentration with height (Fig. 11) is similar to observations made during Project Shower by Squires and Warner (1957). The average drop concentration at 1 km was about 70 cm^{-3} , decreasing to 30 cm^{-3} at 1.6 km. In the model at 25 min, the maximum concentration (47 cm^{-3}) occurred near the 1 km level and decreased upward. At 1.5 km, it was 40 cm^{-3} . There was

a sharp decrease in concentration near the cloud top.

Considerable differences exist between calculated and observed values of liquid water content. The ratio of the observed liquid water content to the adiabatic value, presented by Warner (1955), decreases with height. The mean ratio, near cloud base, was 0.5 dropping to 0.2 at 1 km above cloud base. Numerical model results, however, show the ratio near cloud base (at 30 min) to be 0.8, gradually increasing with height to 1.0 at 1 km above cloud base. This discrepancy may be caused partly by the unrealistic lack of mixing with environmental air in the model and partly by the difficulty of accurately measuring in-cloud liquid water content as a function of time and space.

The occurrence in the model of minimum salt content in the upper portions of clouds is in good agreement with the observations of Komabayasi and Isono (1967).

With regard to the salt content in rainwater, the results obtained with the present model differ slightly from the observations of Turner (1955) and the results of Takahashi (1976a). Both investigators indicate that minimum salinity is associated with the heaviest rainfall. The present study, however, shows that the heaviest rainfall, occurring at 44 min, is associated with relatively

high salt content, while the secondary peak in rainfall intensity at 52 min coincides with minimum salt content.

The drop size distribution at 1.8 km (at 30 min) may be compared with results reported by Brown and Braham (1959) who made observations in the Bahamas. For drops of 200 μm in radius, the observed concentration near the cloud top was $10^4 \text{ mm}^{-1} \text{ m}^{-3}$. In the model it was $7 \times 10^4 \text{ mm}^{-1} \text{ m}^{-3}$, about an order of magnitude greater than the observed value.

It is important to consider the relative accuracy of the calculation schemes employed in the present model, which is basically the same model used previously by Takahashi (1973). While the model conserves water content to within about 10 %, both the number of particles and drops and the mass of water are well conserved (to less than 7 %) during microphysical processes.

The time evolution of nucleus spectra computed by the new scheme may be compared with an analytical solution (Fig. 6). Results show that the total particle concentration and salt content are well conserved, and the number densities calculated were within 2 %, except near a radius of 0.5 μm where the maximum deviation (7 %) occurred. The time evolution of drop mass density by condensation-collection computed by numerical methods may be compared

with the analytical solution (Fig. 7). Results show that the total drop concentration calculated at 2000 sec differs by only 2 % from that derived from the analytic solution, while the total drop mass differs by 0.7 %. Drop mass densities agree within 3 %.

The space increment used (200 m) may appear to be somewhat large. Previous studies (Ogura and Takahashi, 1973), however, indicate no significant difference in results using the same computational scheme with a 100 m space increment.

The comparison of numerical results with observations in nature reveals that the present model simulates warm cloud development and rainfall reasonably well, and so this model may be used to study the effect of cloud nuclei on the initiation of rain in the warm clouds.

2. Nucleus mass range and number concentration efficient for warm rain development.

The principal results of experiments with different nucleus size distributions and concentrations are summarized in Figs. 30 and 31.

The total rainfall from a given cloud remains almost constant until nuclei of mass greater than 10^{-15} g are removed (Fig. 30). When nuclei of mass greater than 10^{-17} g are removed, the total rainfall decreases sharply.

This suggests that nuclei of mass about 10^{-15} g are the most efficient for warm rain initiation.

When the nucleus concentration is either increased or decreased from a standard value, the resulting total rainfall decreases (Fig. 31). While a decreased nucleus concentration leads to shallow clouds, an increased concentration produces deep clouds. These deep clouds, however, soon transform into stable continental-type clouds, characterized by numerous small droplets. These results suggest that the standard nucleus concentration yields the maximum total rainfall.

The nucleus concentration observed near the coastline of Hilo, Hawaii, fluctuates, depending on atmospheric conditions. Based on Squires' (1958) cloud droplet observations and Jiusto's (1967) nuclei measurements, it appears that the nucleus concentration may vary from about one-fifth to five times the standard concentration. Within this wide range the total rainfall does not vary significantly from the maximum total rainfall (Fig. 31).

3. Application.

Cloud model results indicate that the cloud nucleus size distribution and concentration affect the development of warm clouds and rainfall only in extreme cases. The rapid addition of large numbers of nuclei, as sometimes

observed in Hawaii (sugar cane field burning and volcanic eruptions), suppresses in-cloud drop growth. Rainfall may not develop in such clouds, or if it does rain, the amount will be substantially reduced. For example, if the nucleus concentration increased to 20 times the standard concentration, the rainfall amount would be reduced by about 50 %.

Suppose giant nuclei were used to seed non-precipitating warm clouds to induce rainfall. Large drops are assumed to form on giant nuclei and initiate the collection process. According to the present results, however, giant nuclei are not essential for raindrop formation so that seeding with such nuclei may be useless. The only effect would be an increase in nucleus concentration and transformation of the cloud into a pseudo-continental type with enhanced cloud stability. The probability of rainfall would be very slight under these conditions.

At the other extreme, cloud nuclei may be substantially reduced by scavenging after rainfall of long duration. With fewer nuclei clouds cannot develop to great heights so that only weak rain occurs, as shown in the present model.

Since the nucleus spectrum usually observed in Hawaii is the most efficient for the development of warm rain, it

is doubtful that more rainfall could be obtained by spraying water drops into the cloud top. Takahashi (1976b) demonstrated with numerical modeling that only continental warm cloud rainfall could be increased by such spraying. Thus, it appears that warm clouds will be difficult to modify by changing cloud microphysics.

Rainfall amounts over broad areas may be increased by enlarging the cloud population or by weakening or eliminating the inversion. When clouds become deeper, as observed near the equator, rain forms at high nucleus concentrations since there is ample time for drop growth during upward motions in clouds of great vertical extent.

The present one-dimensional cloud model should be extended to two or three dimensions in the future. This extension will be difficult and may require considerable simplification of microphysics, especially in the nucleus size range.

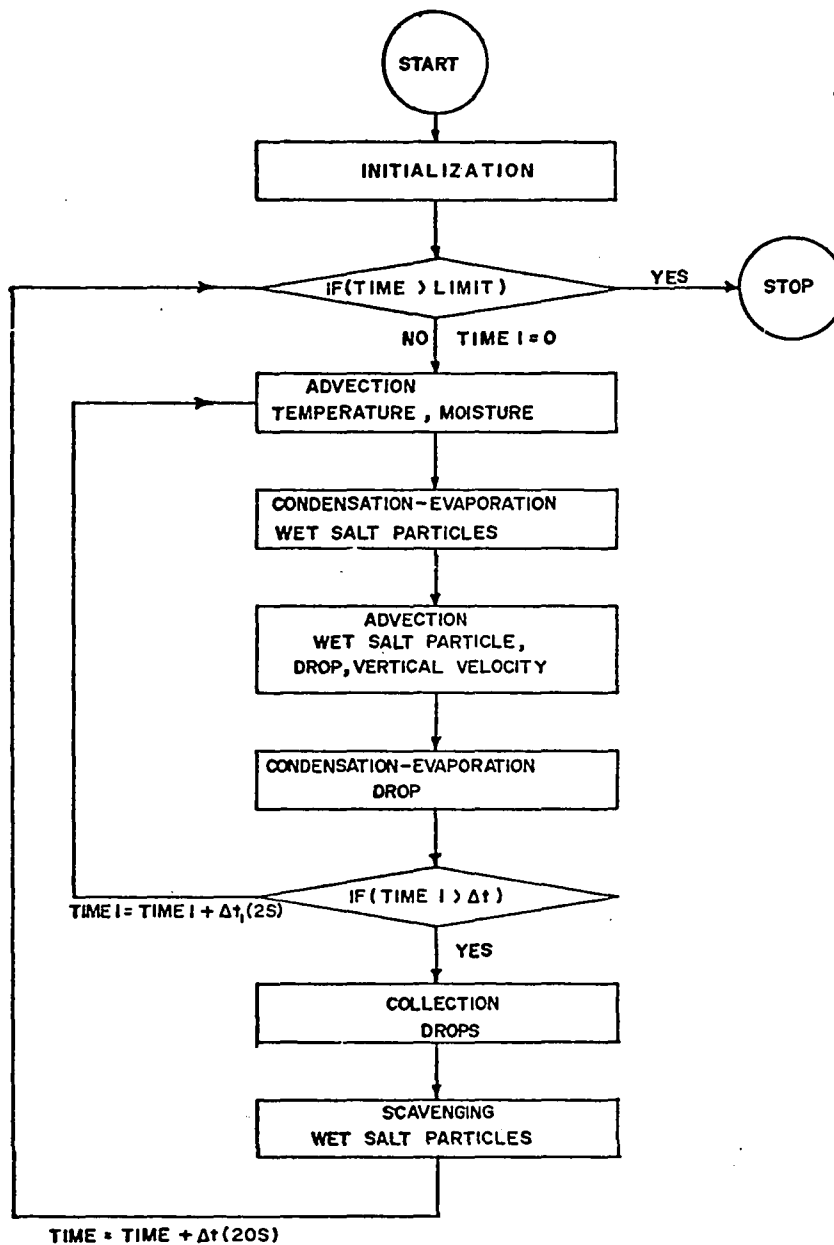


Fig. 2 Flow diagram illustrating the sequence of calculations.

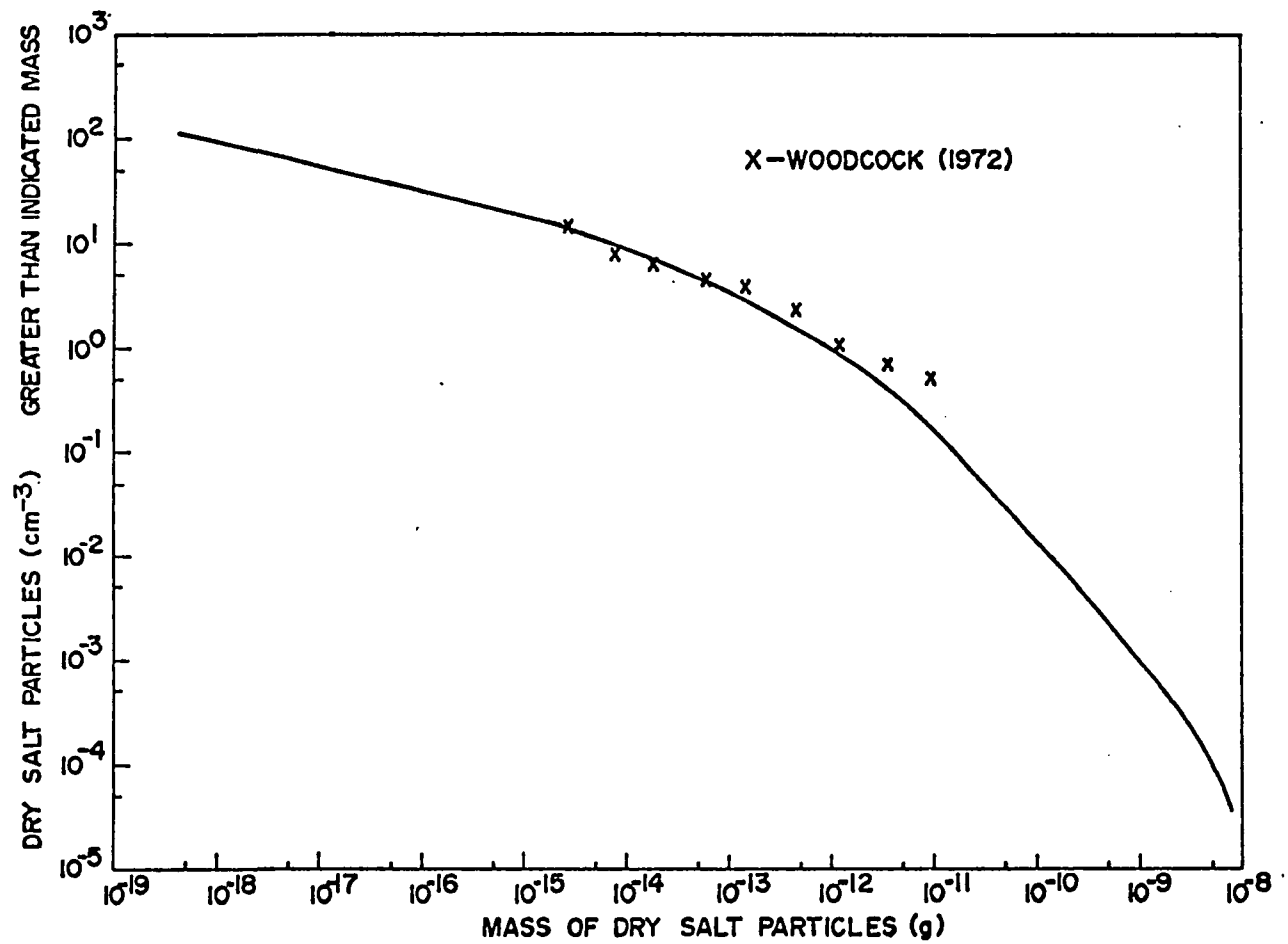


Fig. 3 Dry salt particle concentration in terms of mass. Crosses show the observed values of Woodcock (1972).

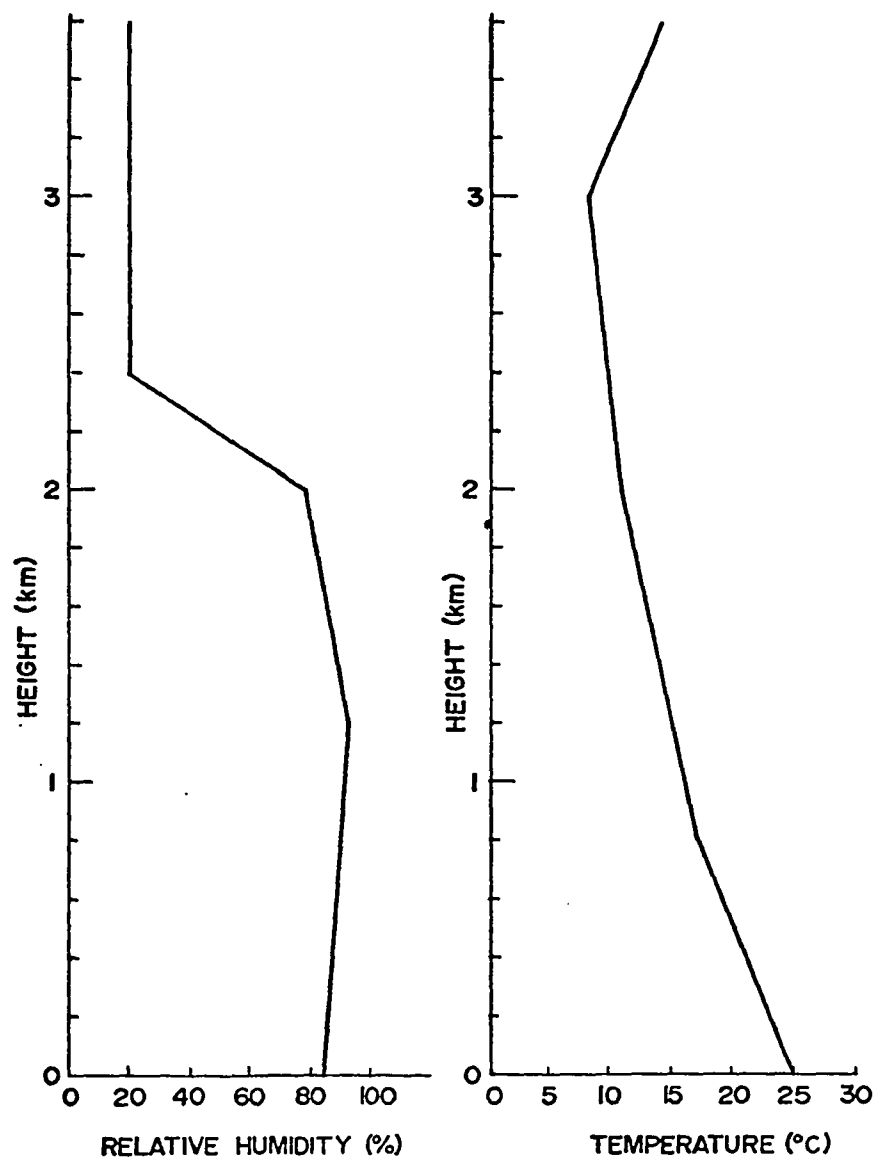
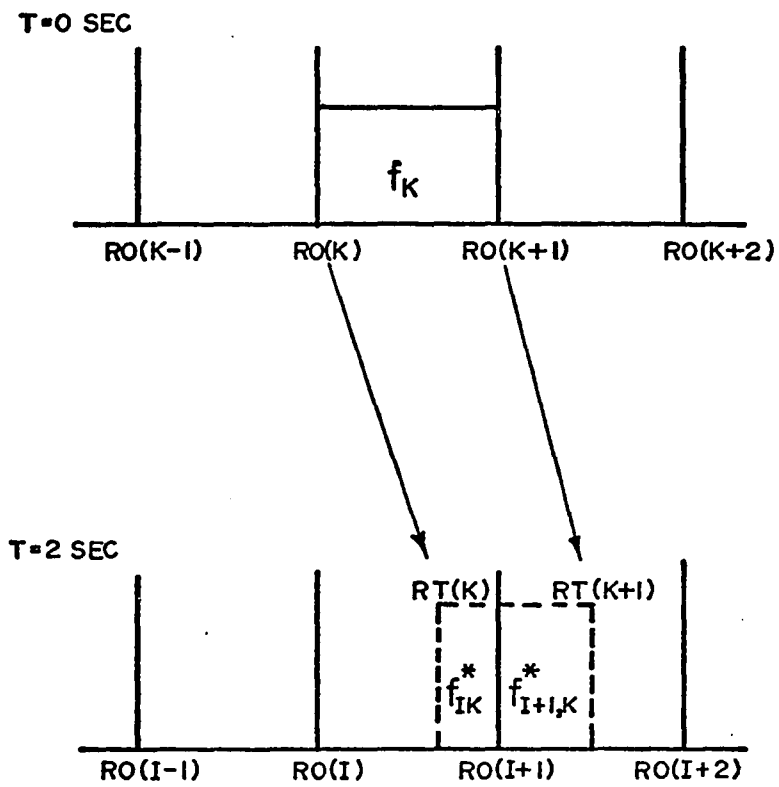


Fig. 4 Environmental temperature and relative humidity profiles.



$$f_{IK}^* = f_K \left[\frac{(RO(I+1) - RT(K))}{(RT(K+1) - RT(K))} \right]$$

Fig. 5 Redistribution of particles after 2 sec growth by condensation.

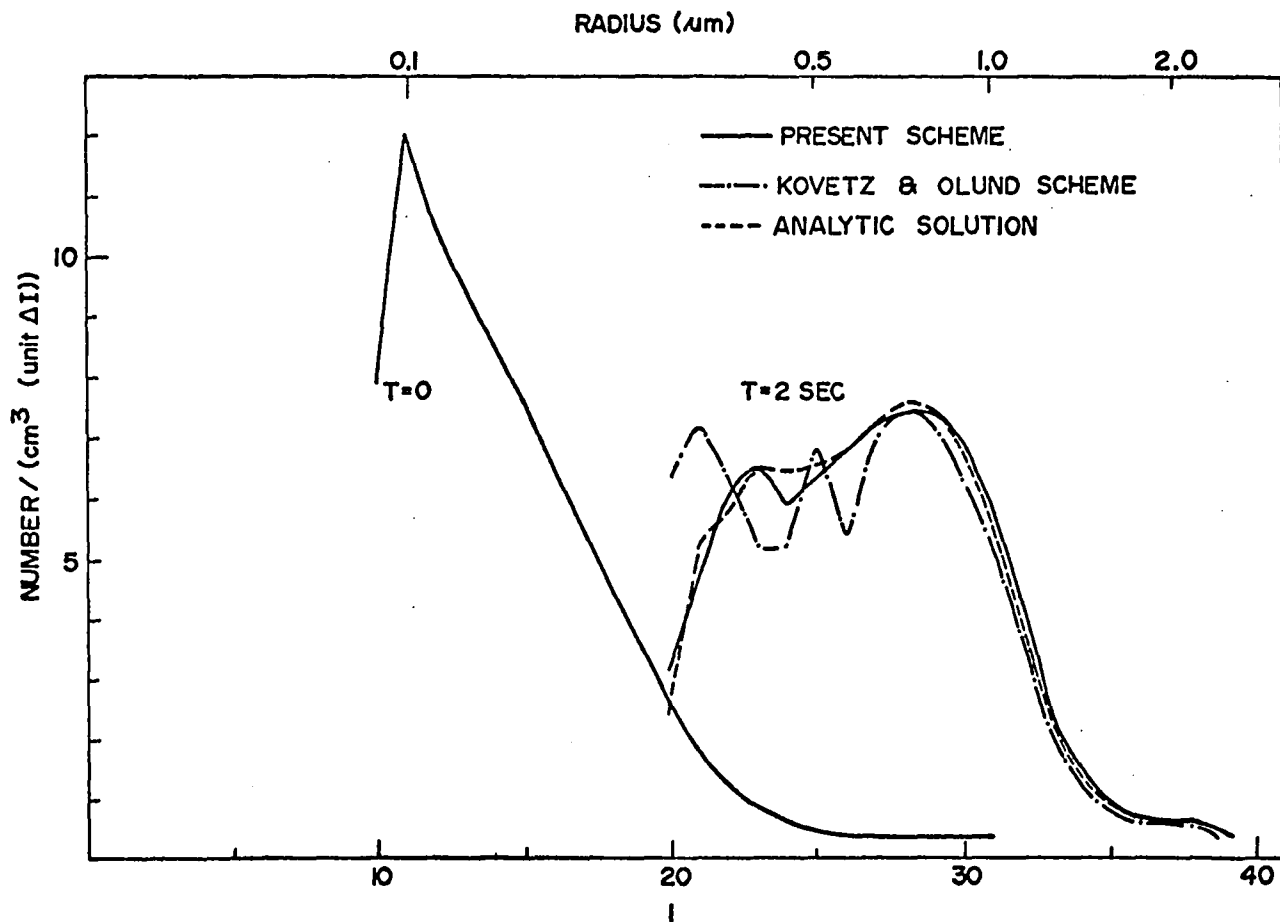


Fig. 6 Time evolution of nucleus spectra by condensation, computed by the present scheme, the Kovetz-Olund scheme and the analytical solution.

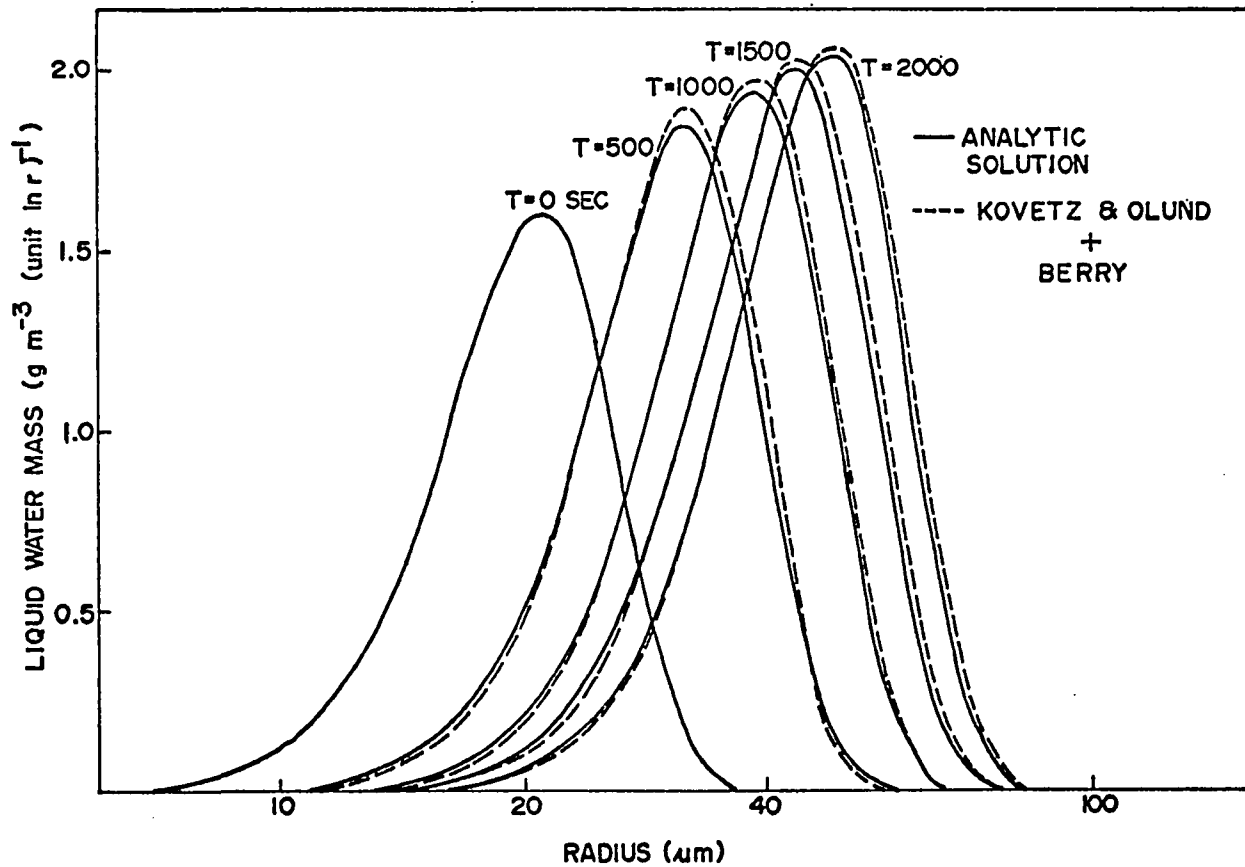


Fig. 7 Time (sec) evolution of the drop mass density by condensation-collection, computed by the combined numerical scheme and the analytic solution.

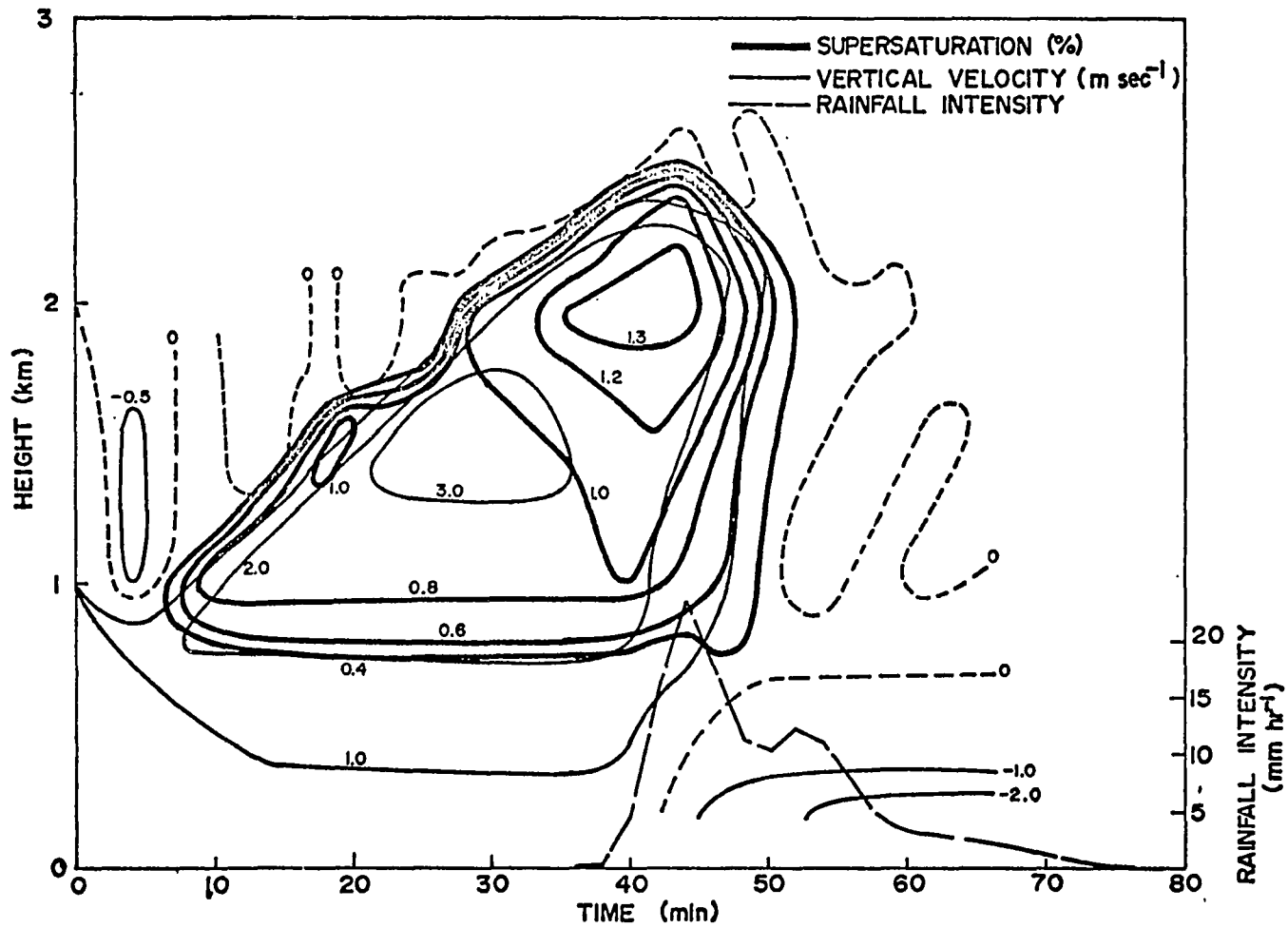


Fig. 8 Time-height variation of vertical velocity and supersaturation for the case of the observed nucleus distribution.

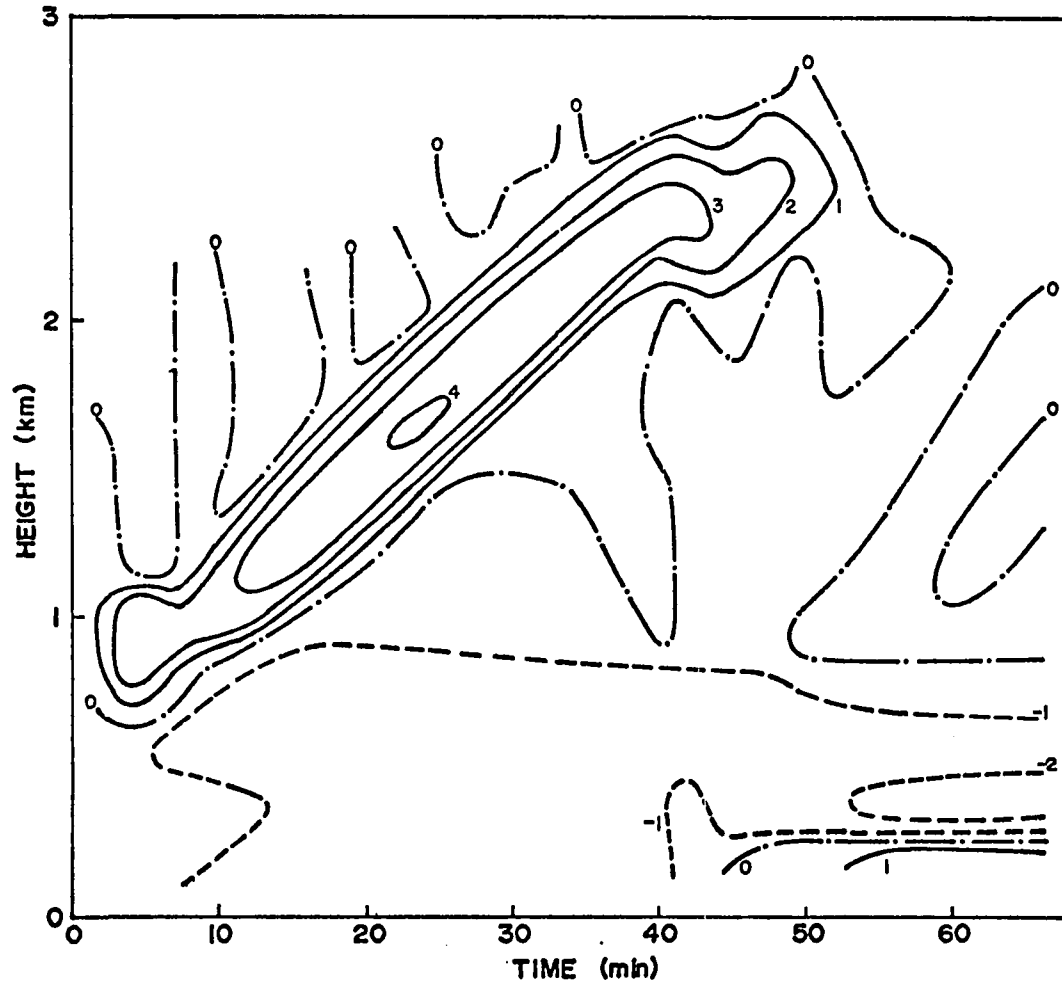


Fig. 9 Time-height variation of radial velocity (m sec^{-1}) for the case of the observed nucleus distribution.

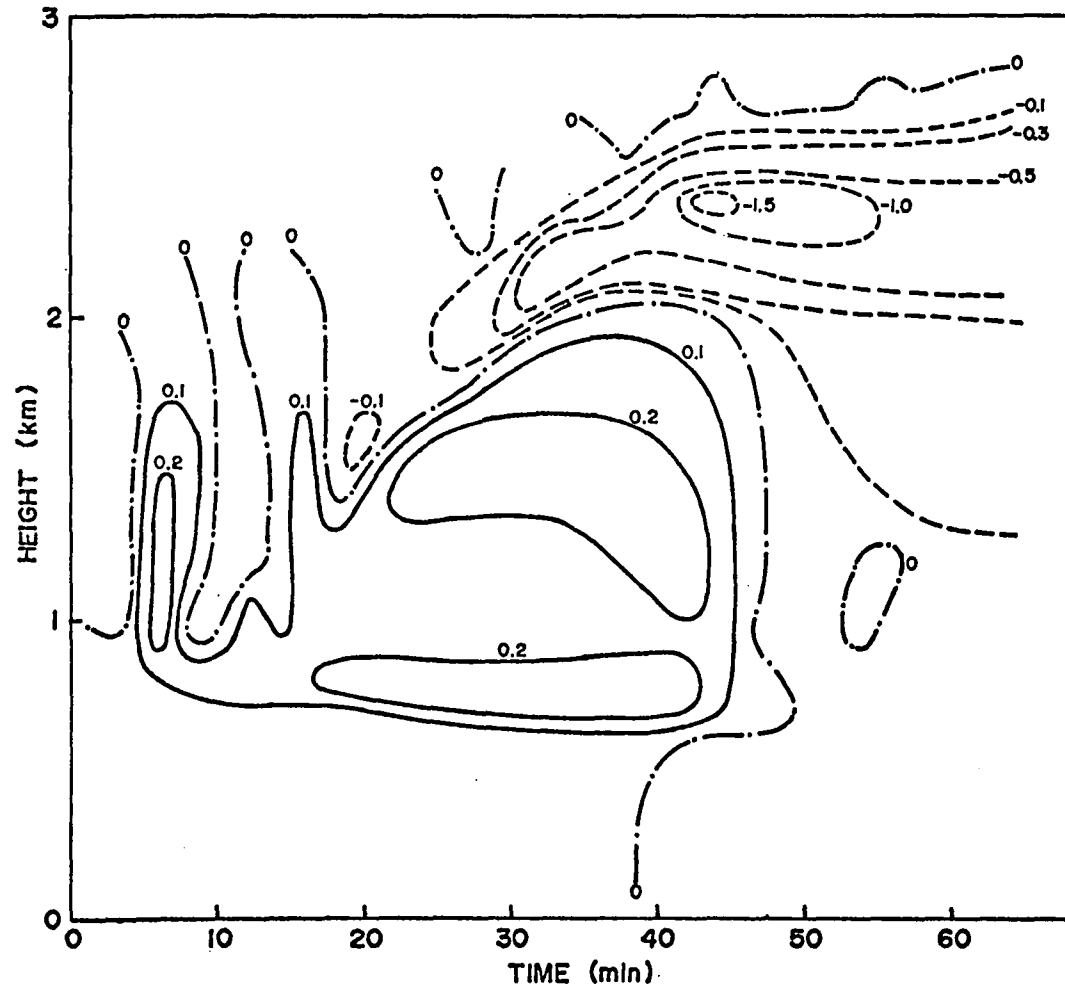


Fig. 10 Time-height variation of temperature differences ($^{\circ}\text{C}$) from environment for the case of the observed nucleus distribution.

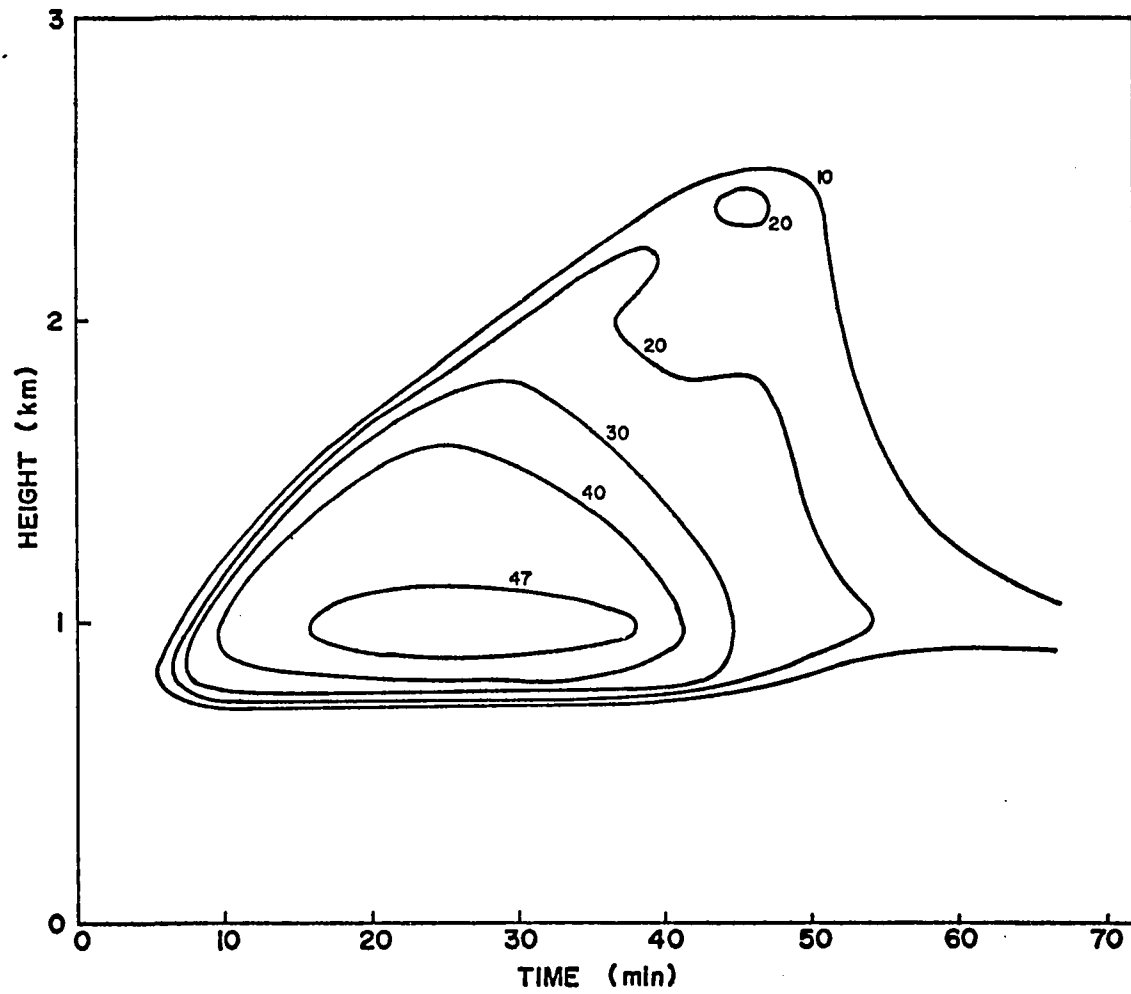


Fig. 11 Time-height variation of drop concentration (cm^{-3}) for the case of the observed nucleus distribution.

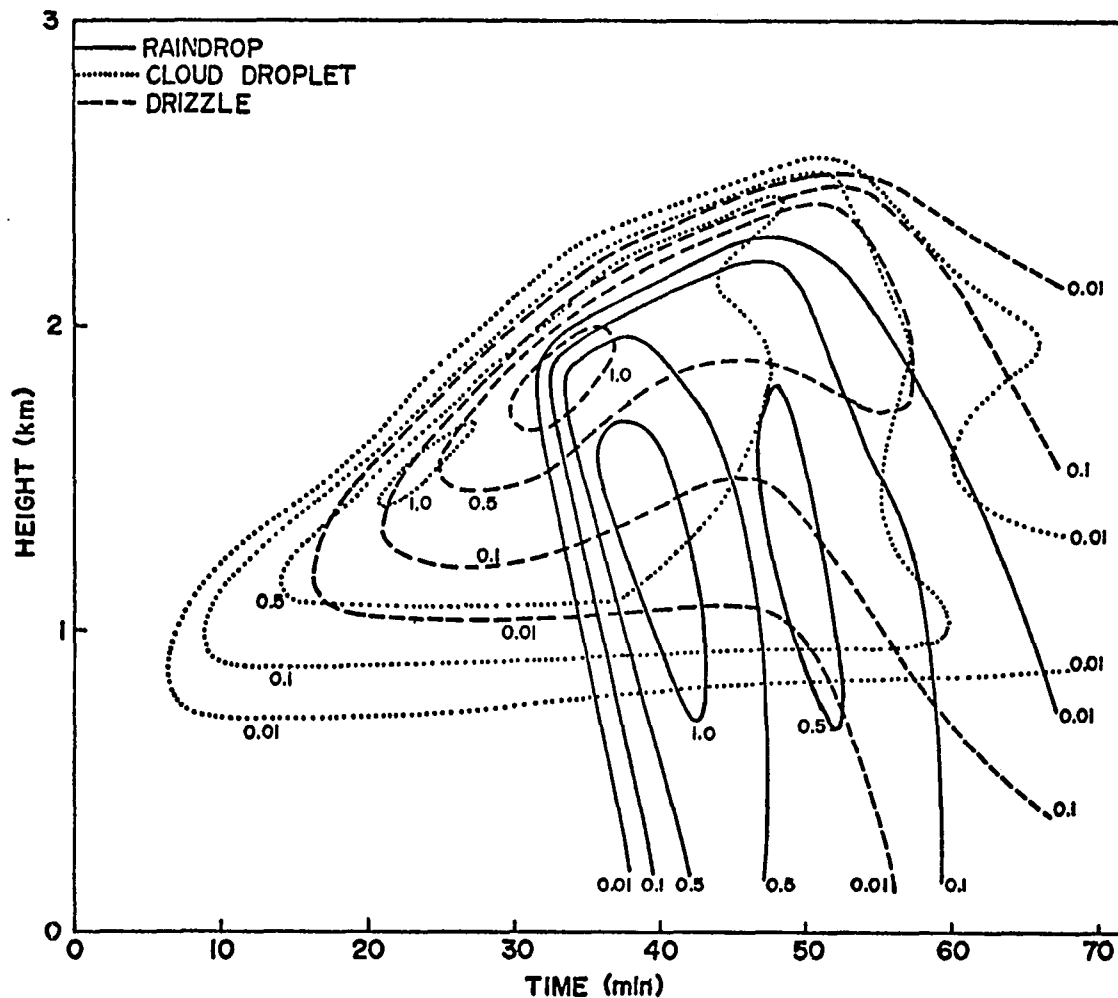


Fig. 12 Time-height variation of the liquid water mixing ratio (g kg^{-1}) for the case of the observed nucleus distribution.

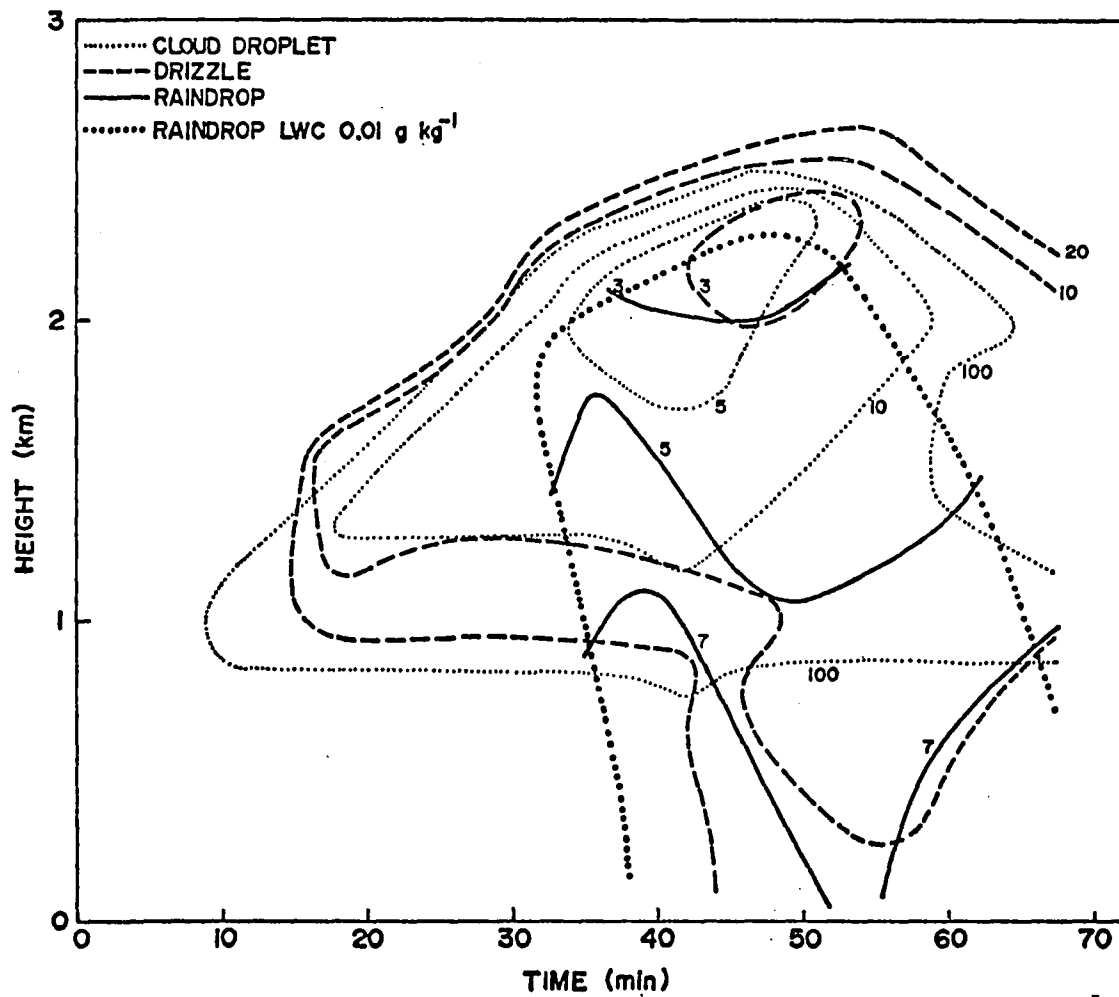


Fig. 13 Time-height variation of salt content (mg l^{-1}) for the case of the observed nucleus distribution.

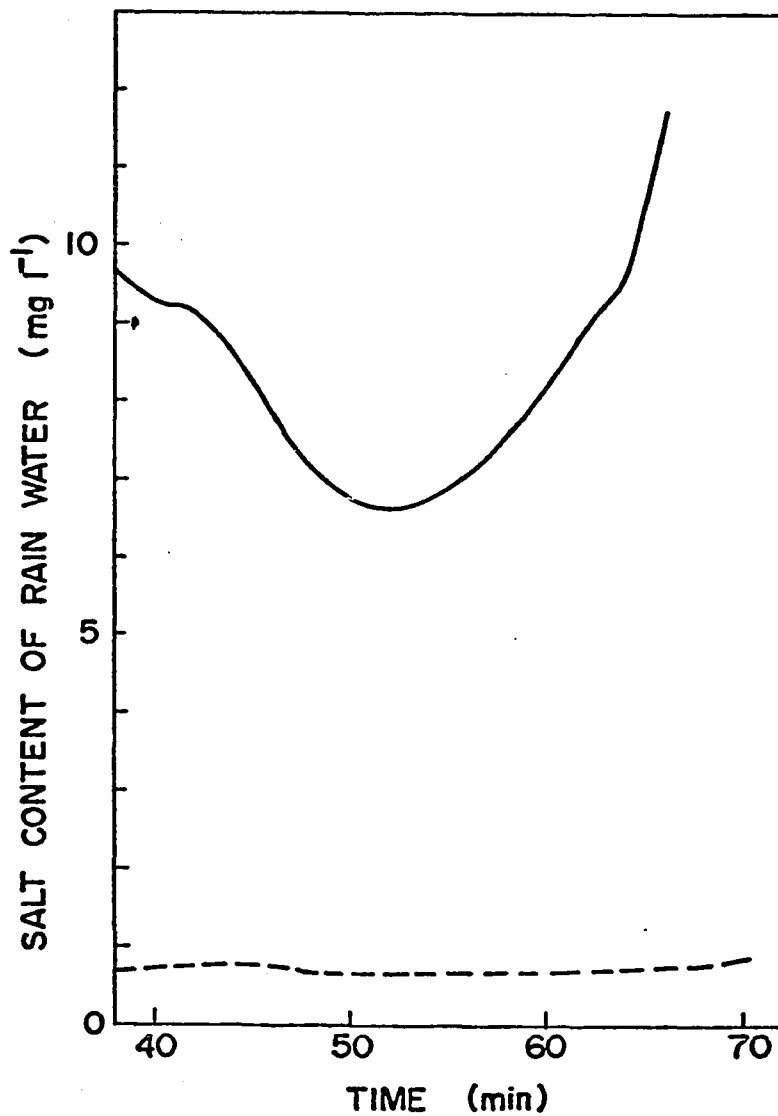


Fig. 14 Time variation of the salt content of rainwater. Solid line is the case with all nuclei; dotted line the case without giant nuclei.

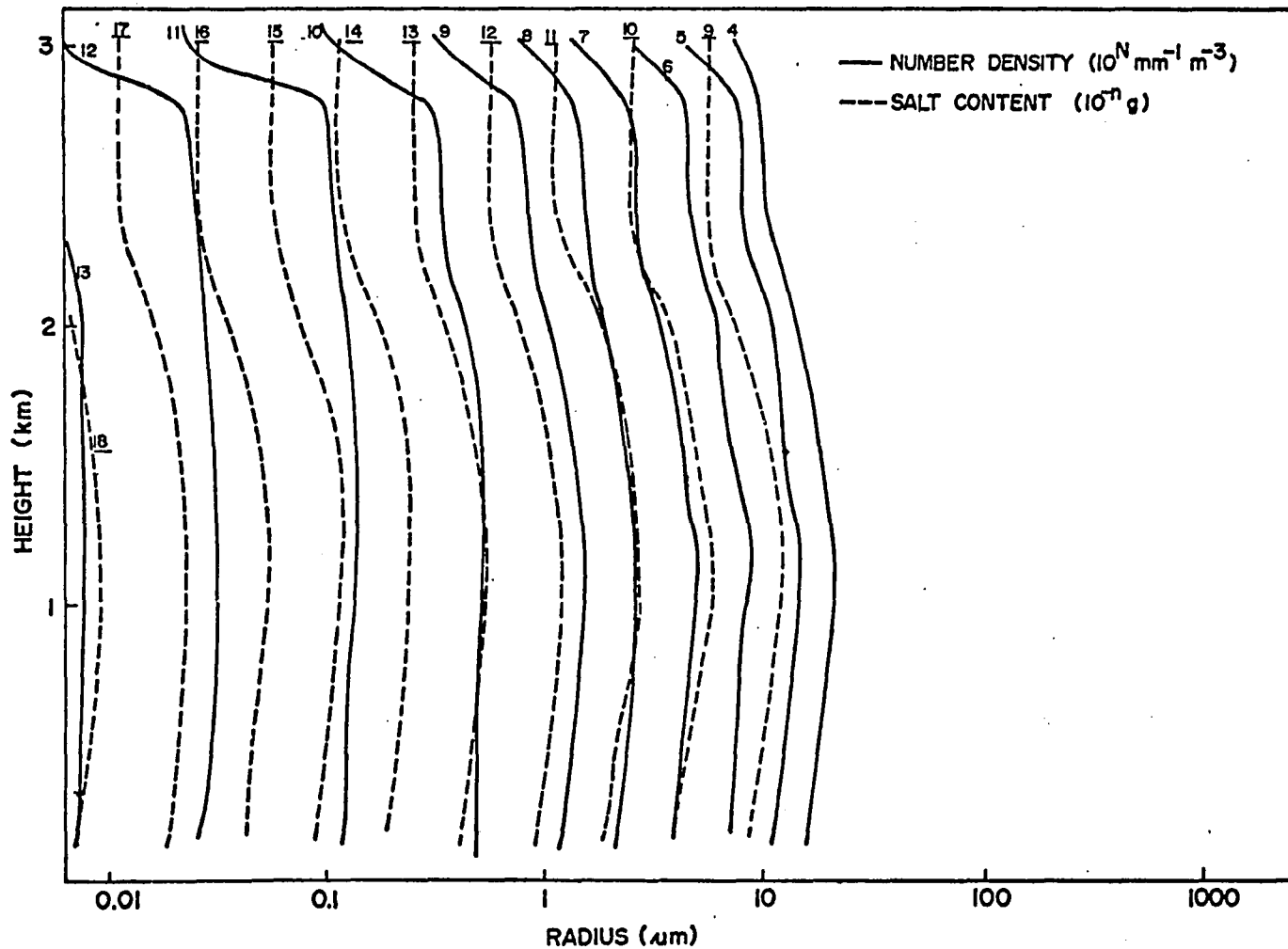


Fig. 15 Wet salt particle and drop density profiles at $t = 0$ with observed nucleus distribution. Number at solid line shows N and underlined number shows n .

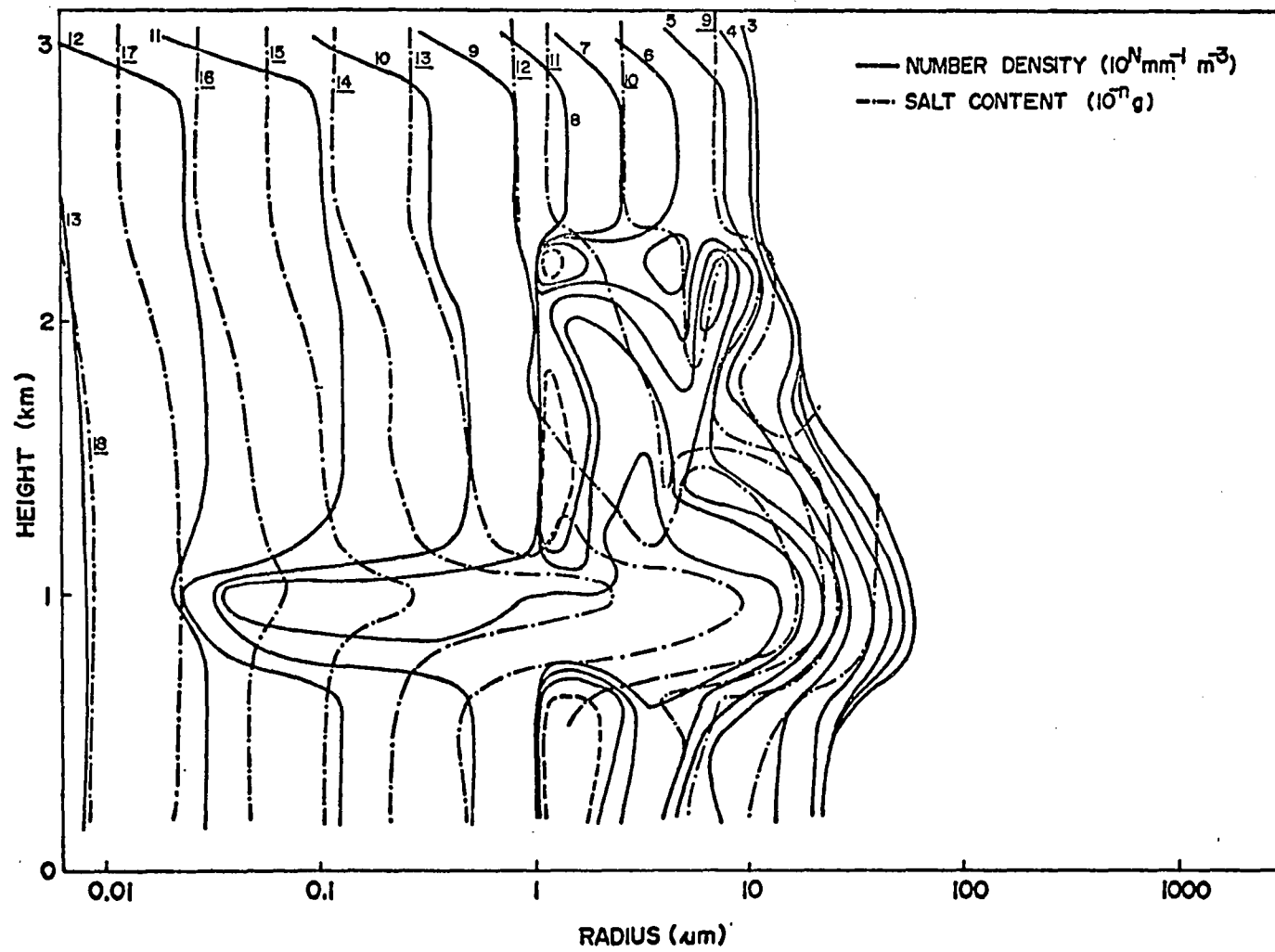


Fig. 16 Same as Fig. 15 except at $t = 10$ min.

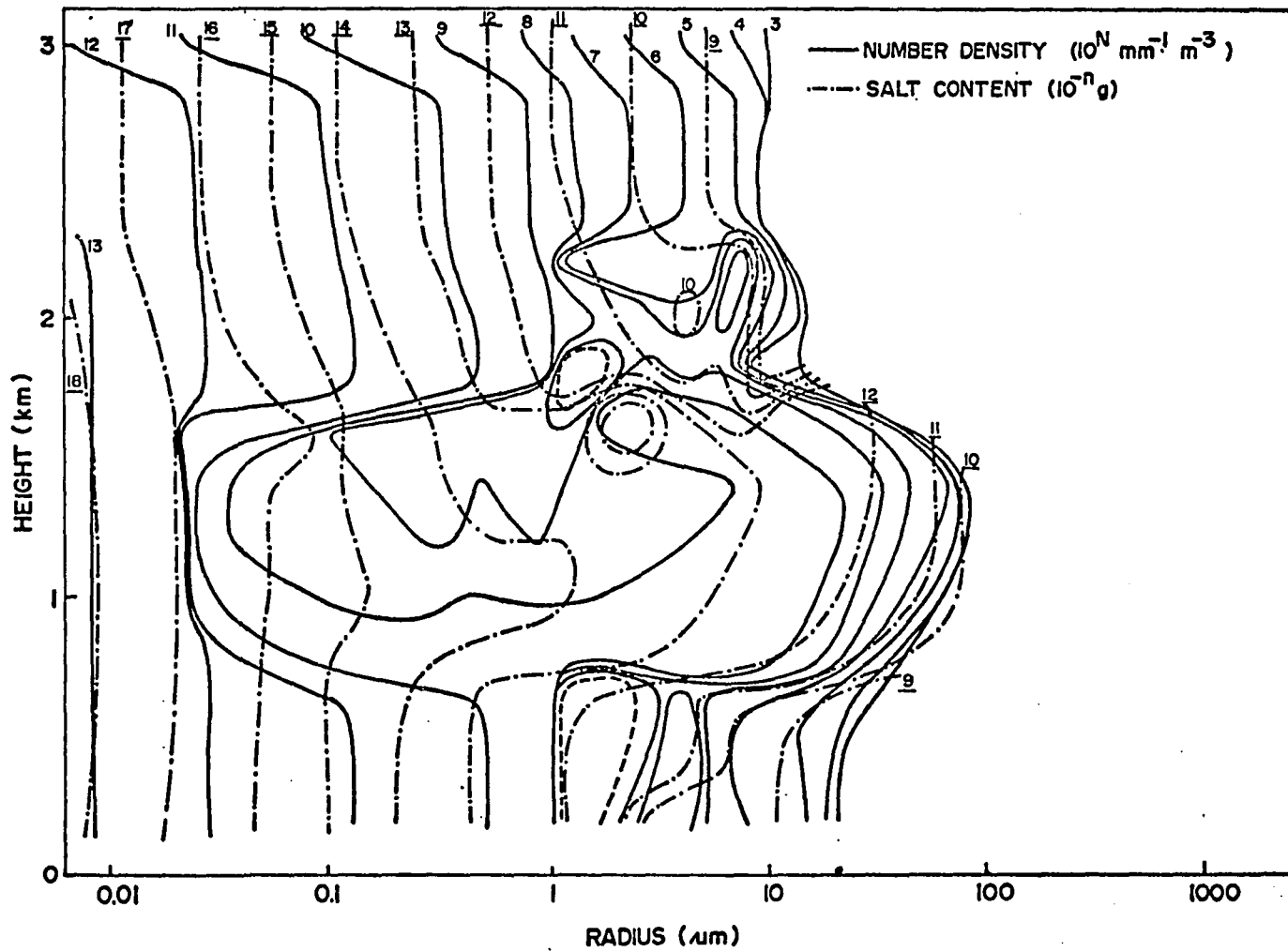


Fig. 17 Same as Fig. 15 except at $t = 20$ min.

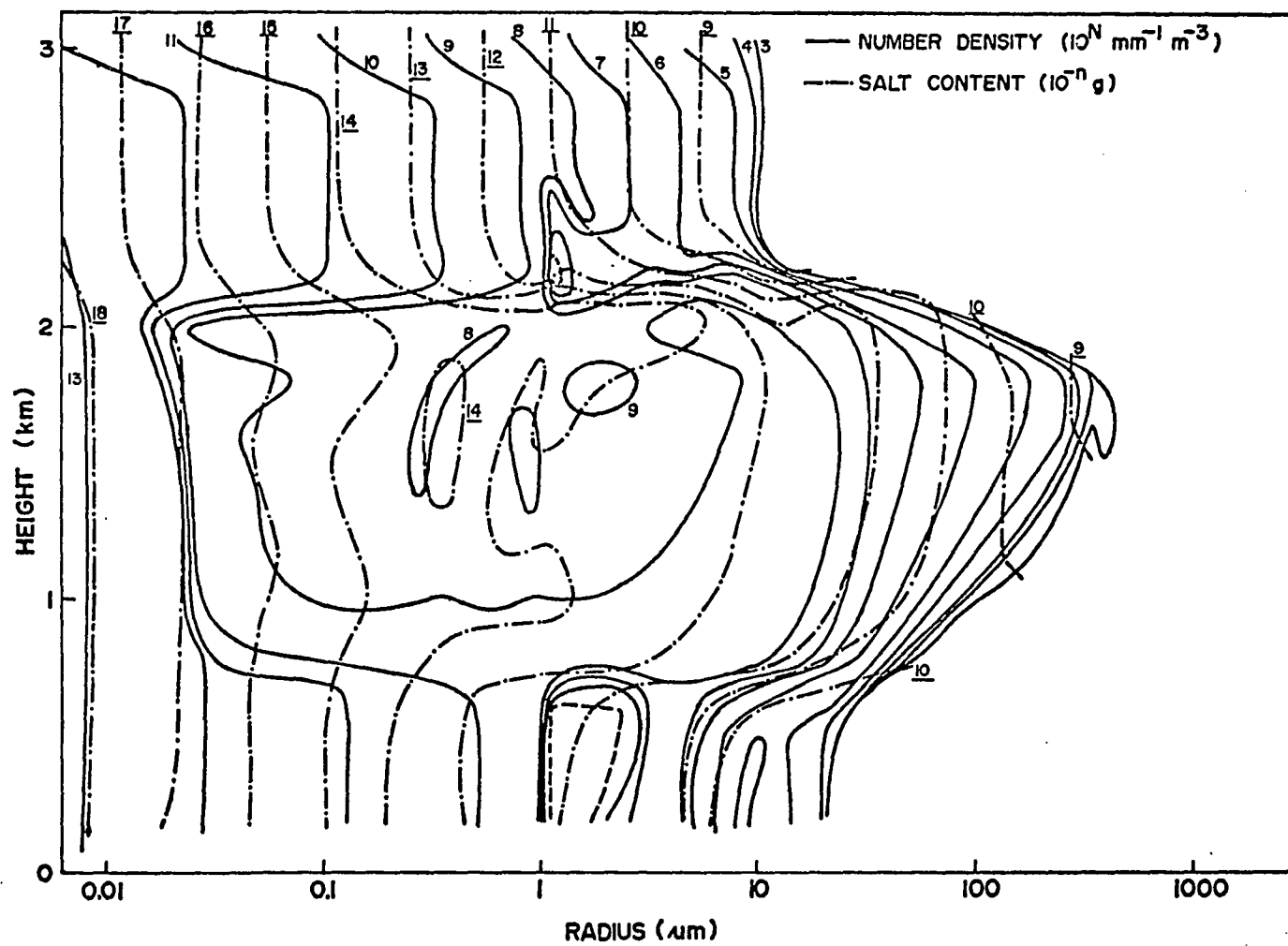


Fig. 18 Same as Fig. 15 except at $t = 30 \text{ min.}$

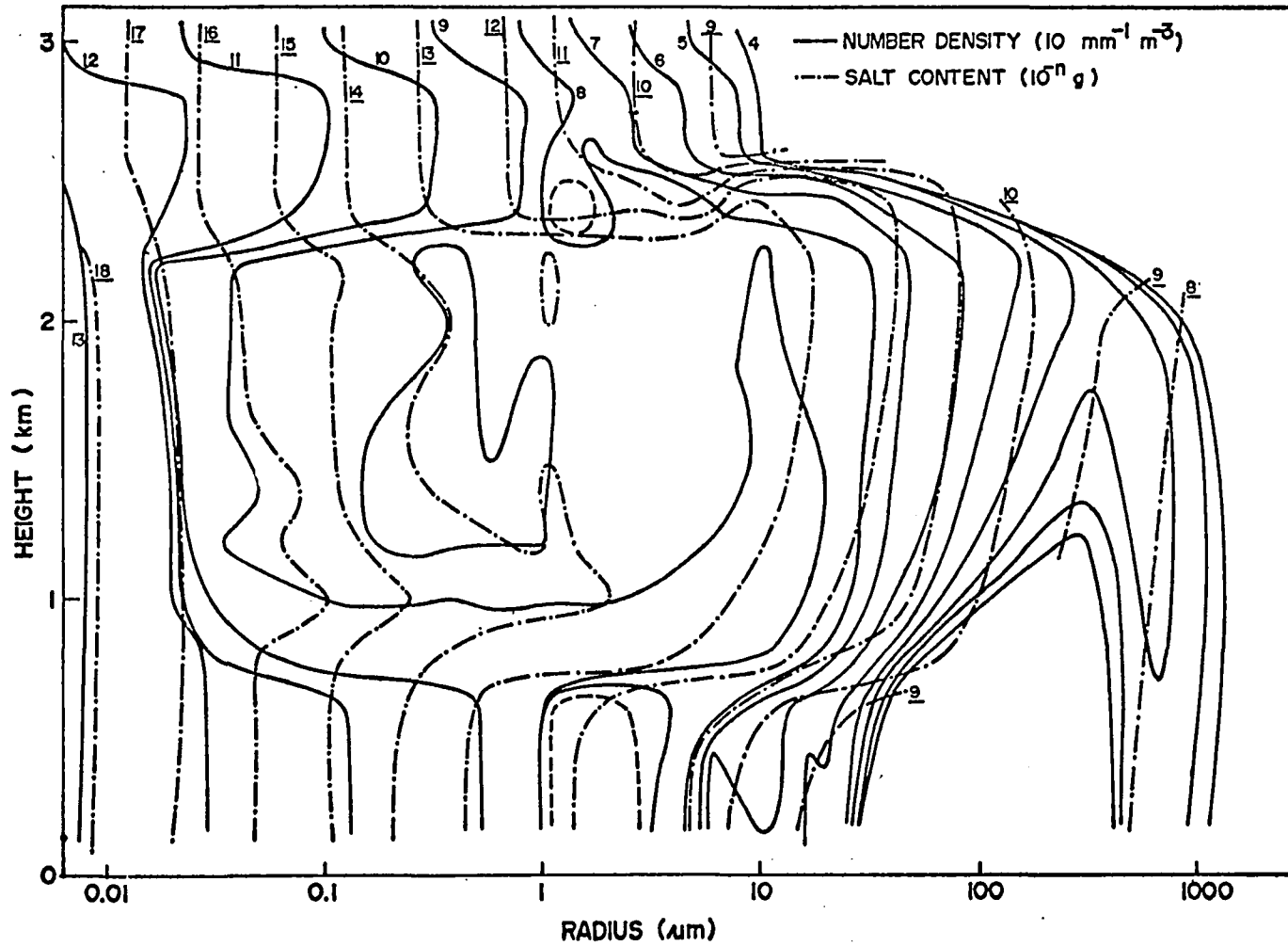


Fig. 19 Same as Fig. 15 except at $t = 40$ min.

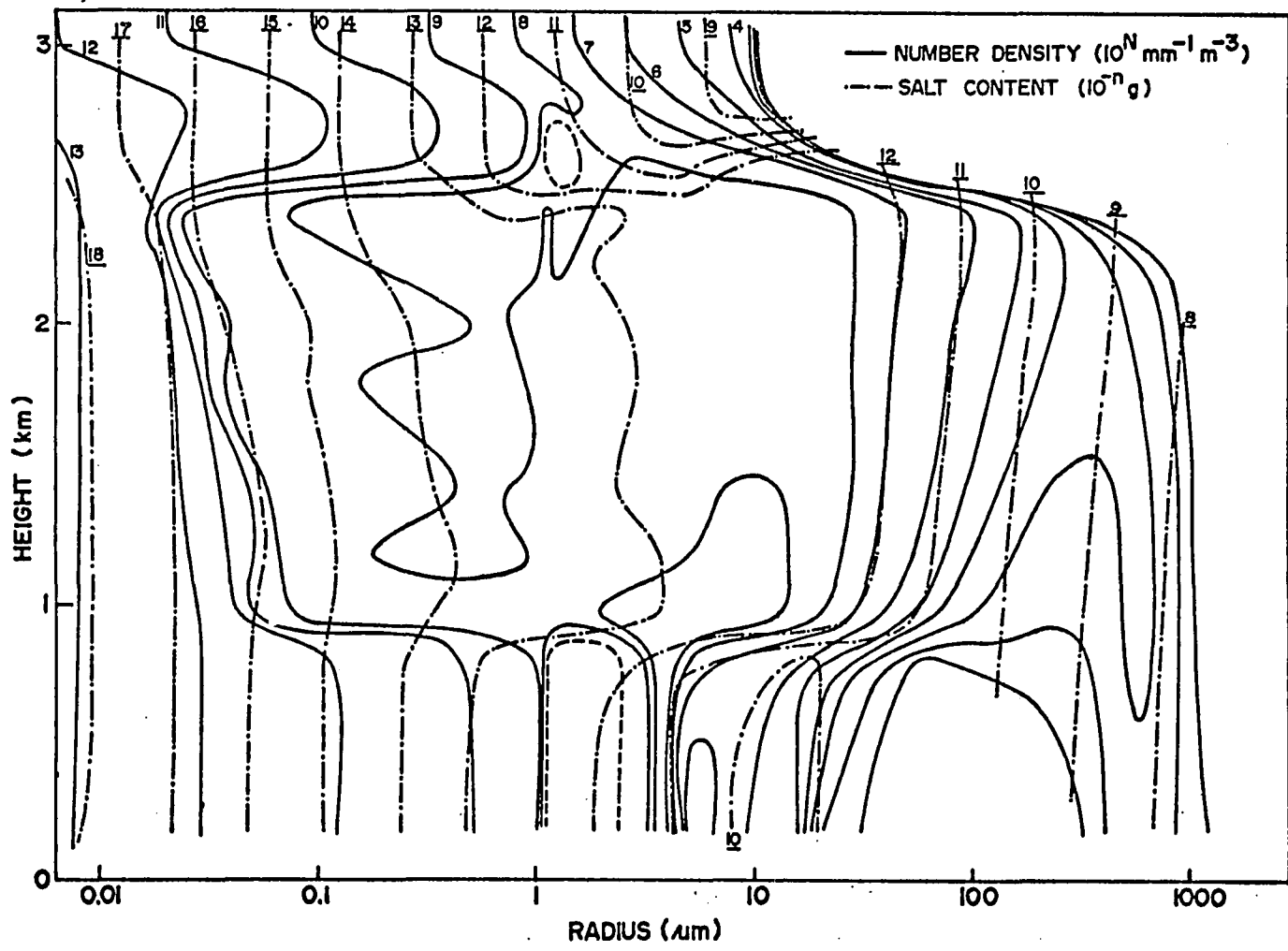


Fig. 20 Same as Fig. 15 except at $t = 50$ min.

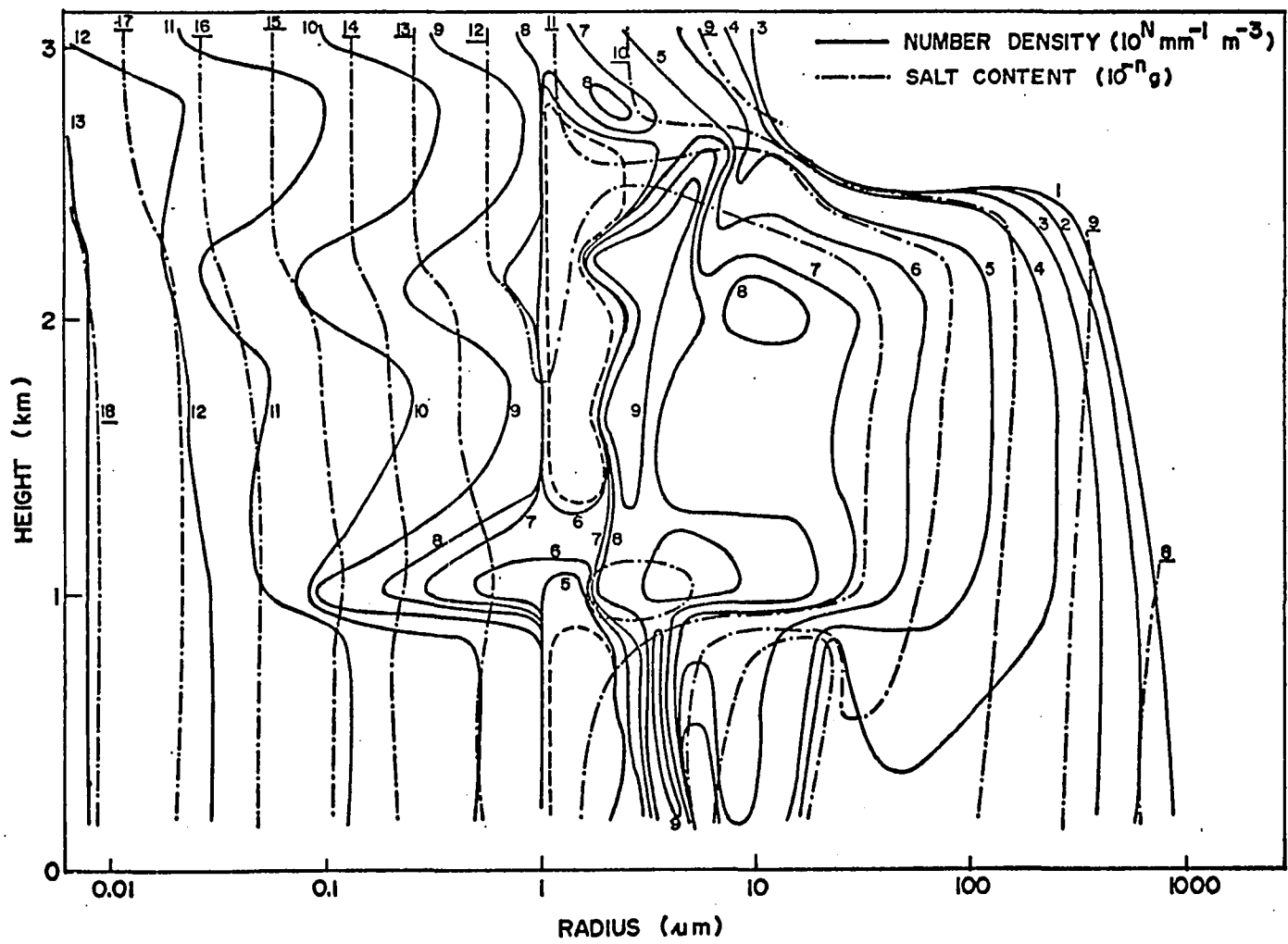


Fig. 21 Same as Fig. 15 except $t = 60$ min.

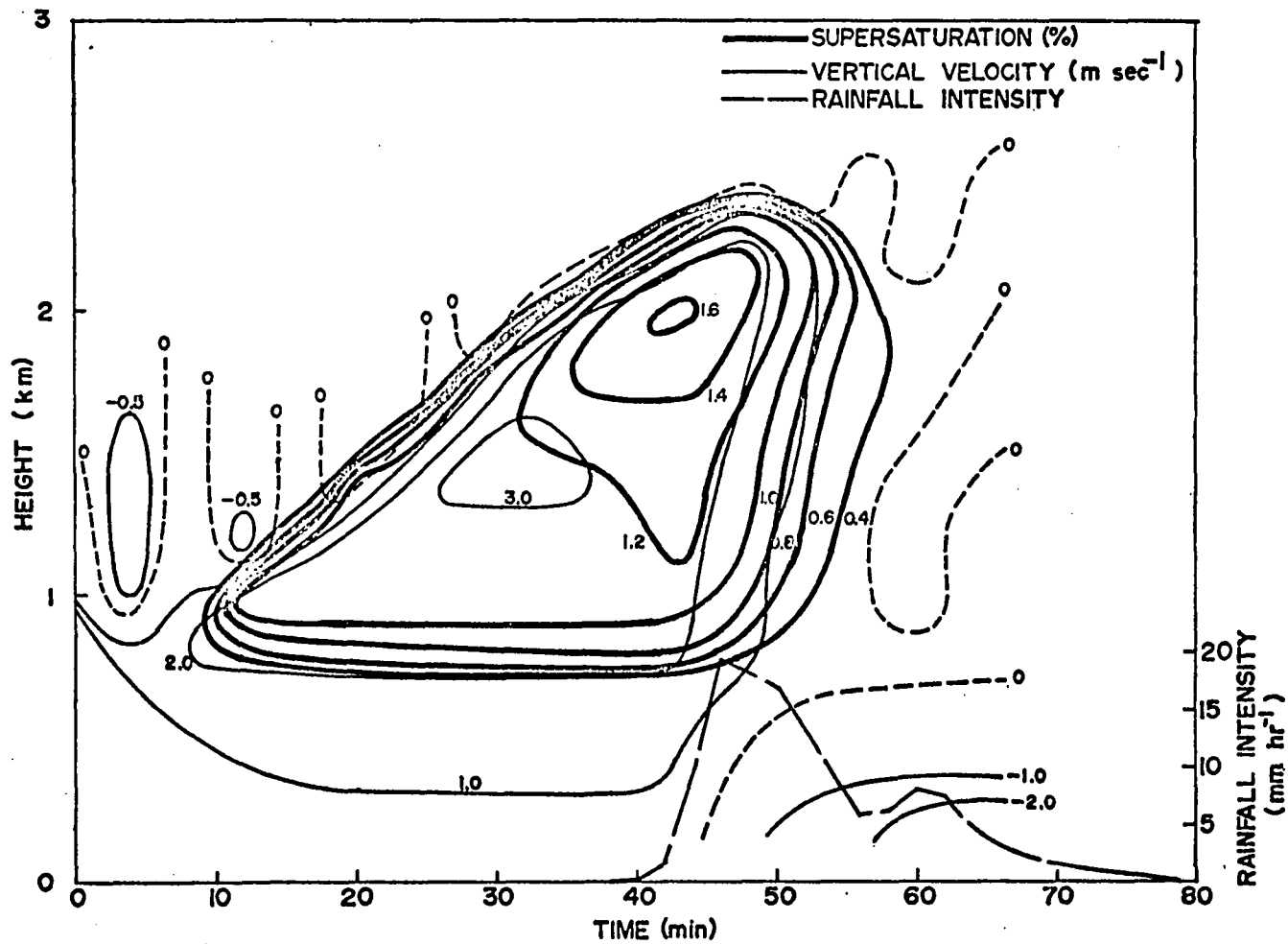


Fig. 22 Time-height variation of vertical velocity and supersaturation for the case of nucleus mass $< 10^{-15}$ g.

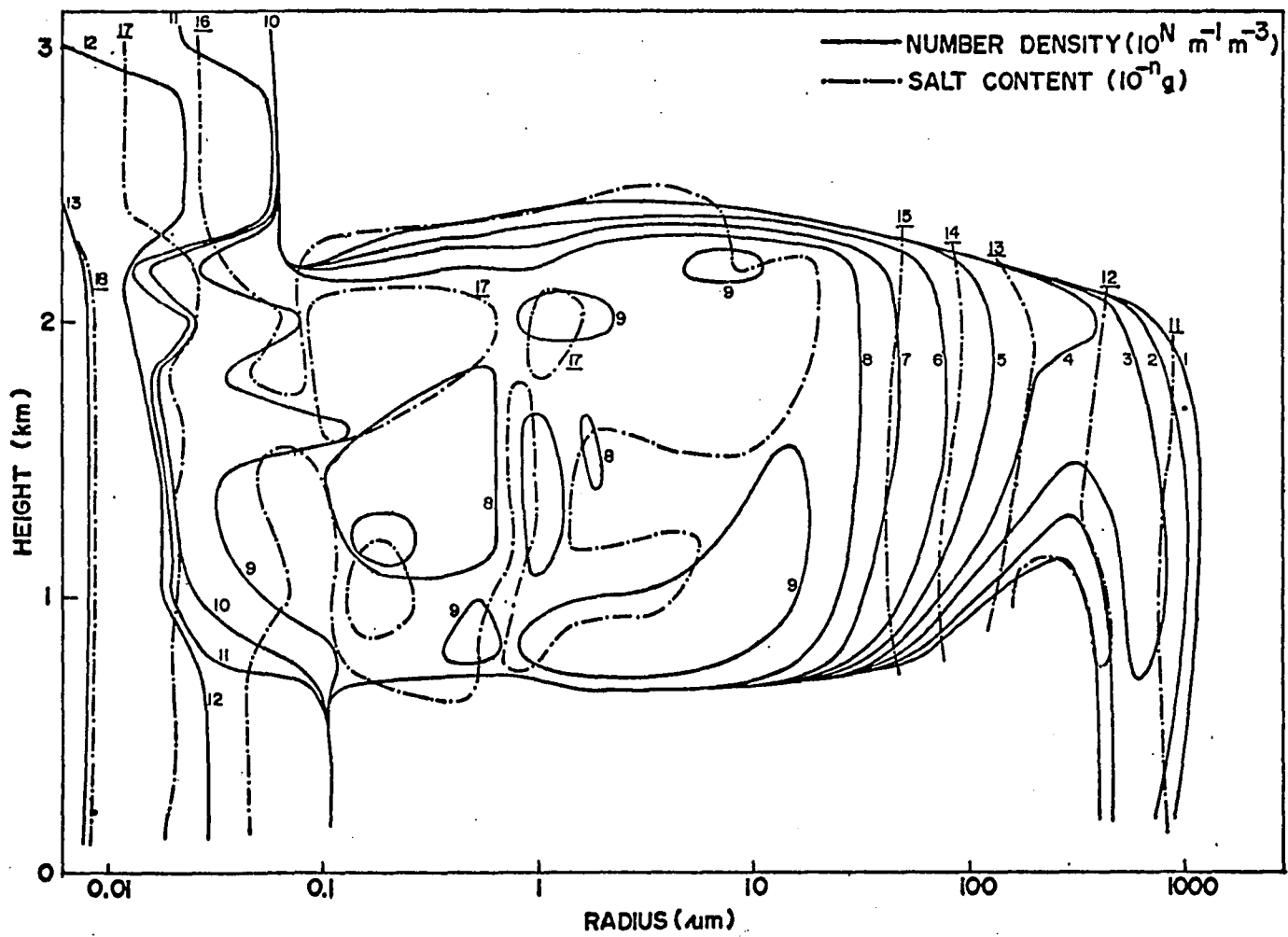


Fig. 23 Wet salt particle and drop density profiles at $t = 42 \text{ min}$, with nucleus mass $< 10^{-15} \text{ g}$. Numbers associated with solid lines show N ; underlined numbers show n .

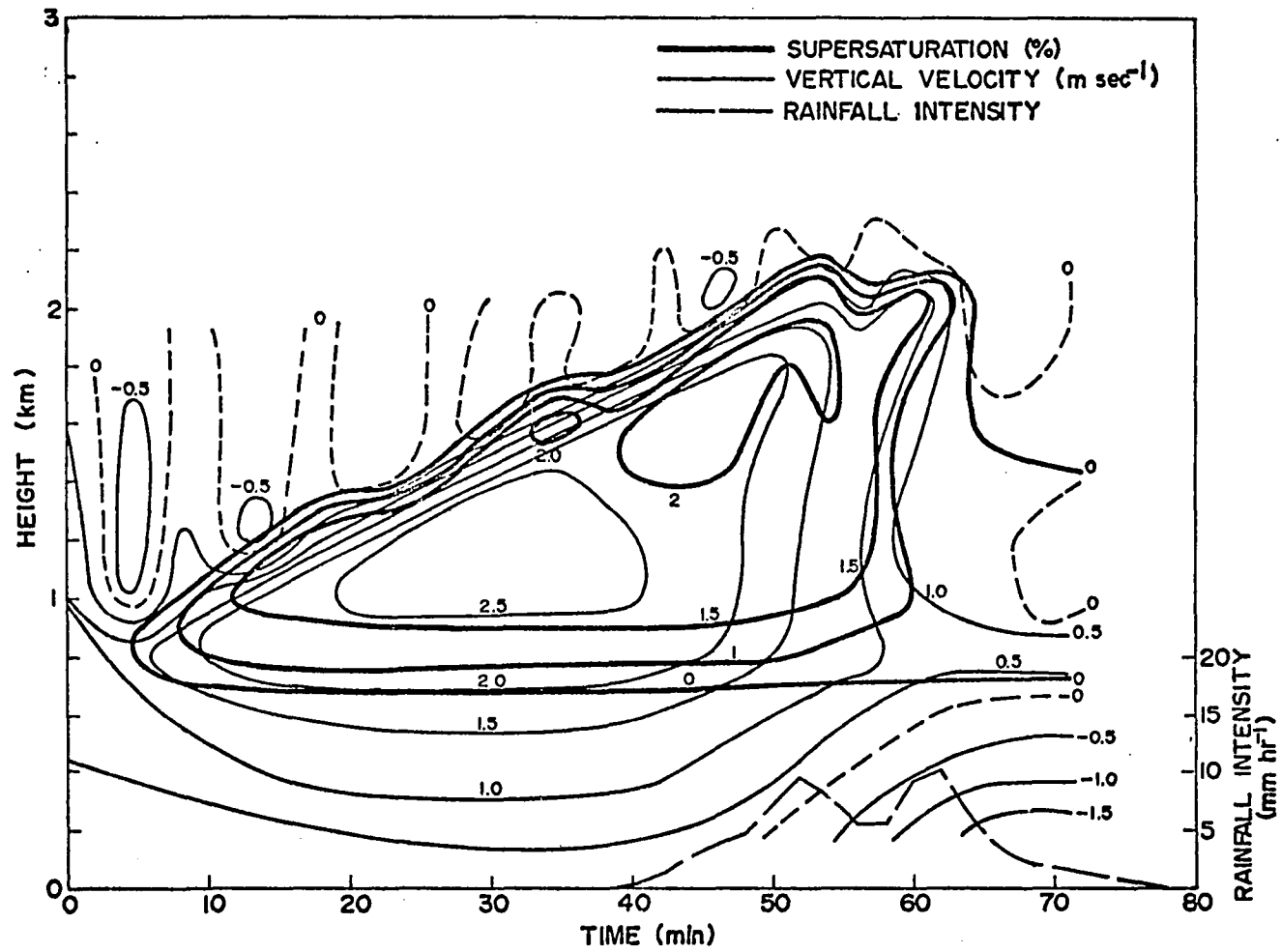


Fig. 24 Time-height variation of vertical velocity and supersaturation for the case of nucleus mass $< 10^{-17}$ g.

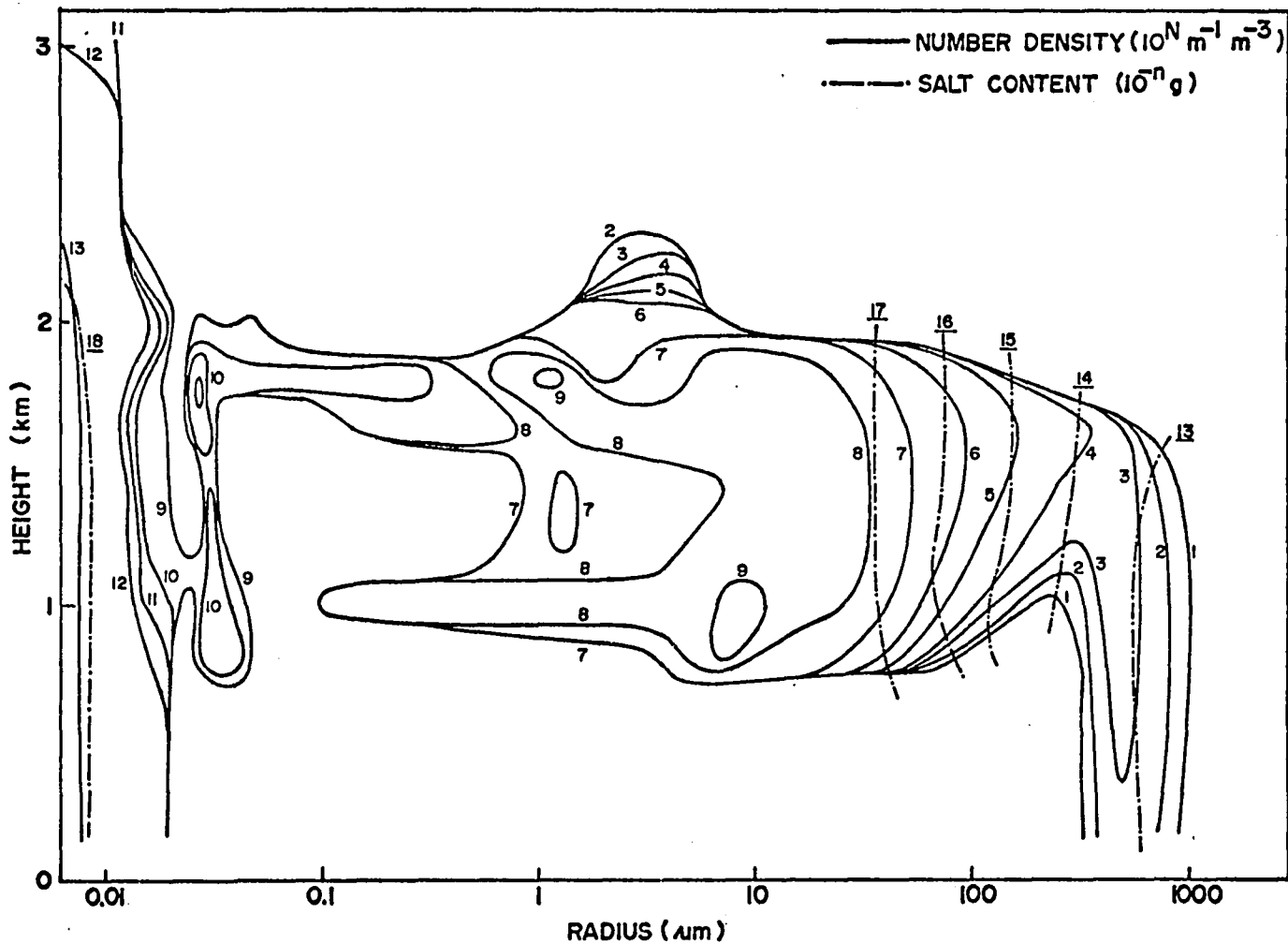


Fig. 25 Wet salt particle and drop density profiles at $t = 44$ min, with nucleus mass $< 10^{-17}$ g. Numbers associated with solid lines show N ; underlined numbers show n .

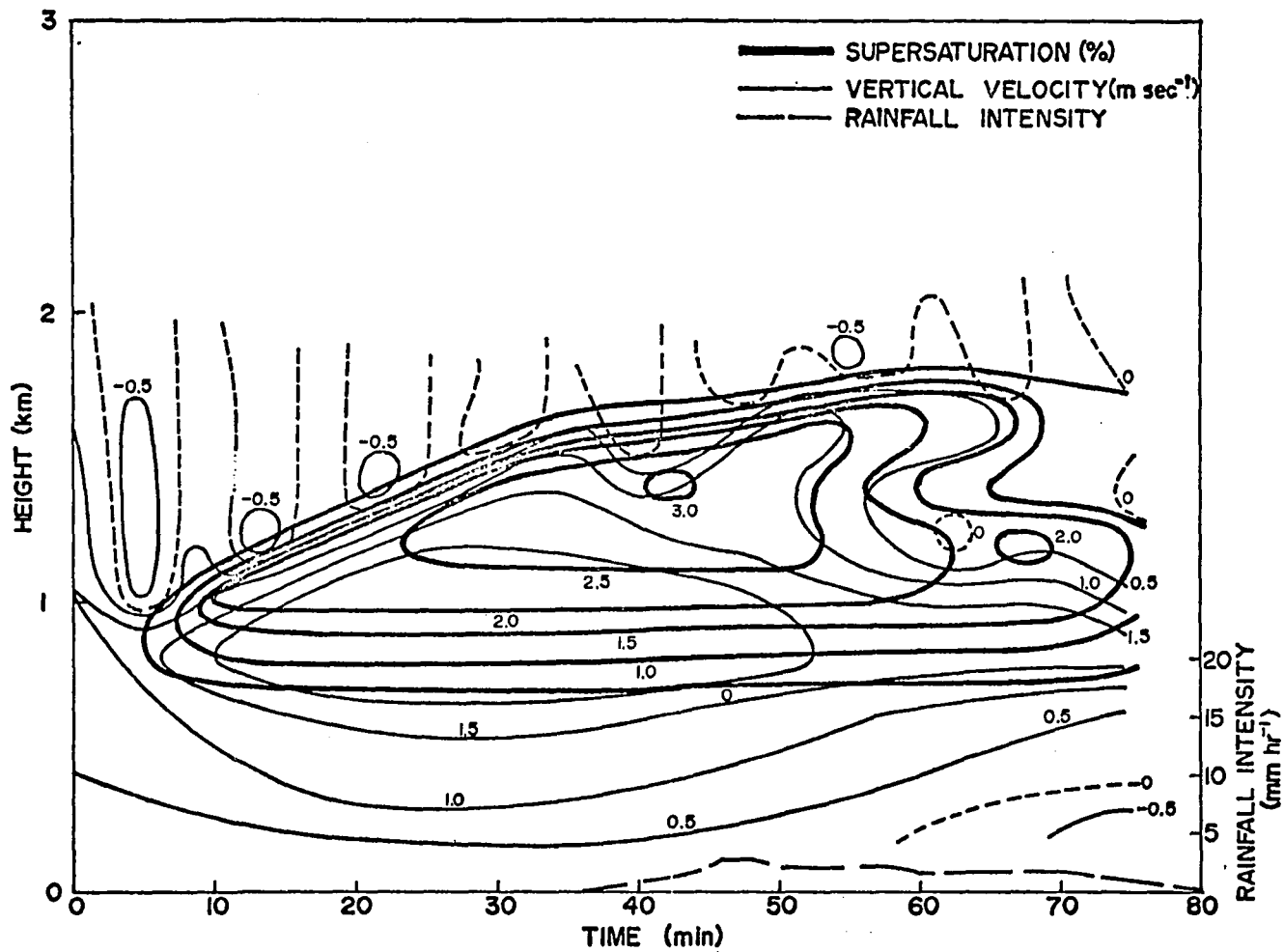


Fig. 26 Time-height variation of vertical velocity and supersaturation for the case of the standard nucleus concentration divided by ten.

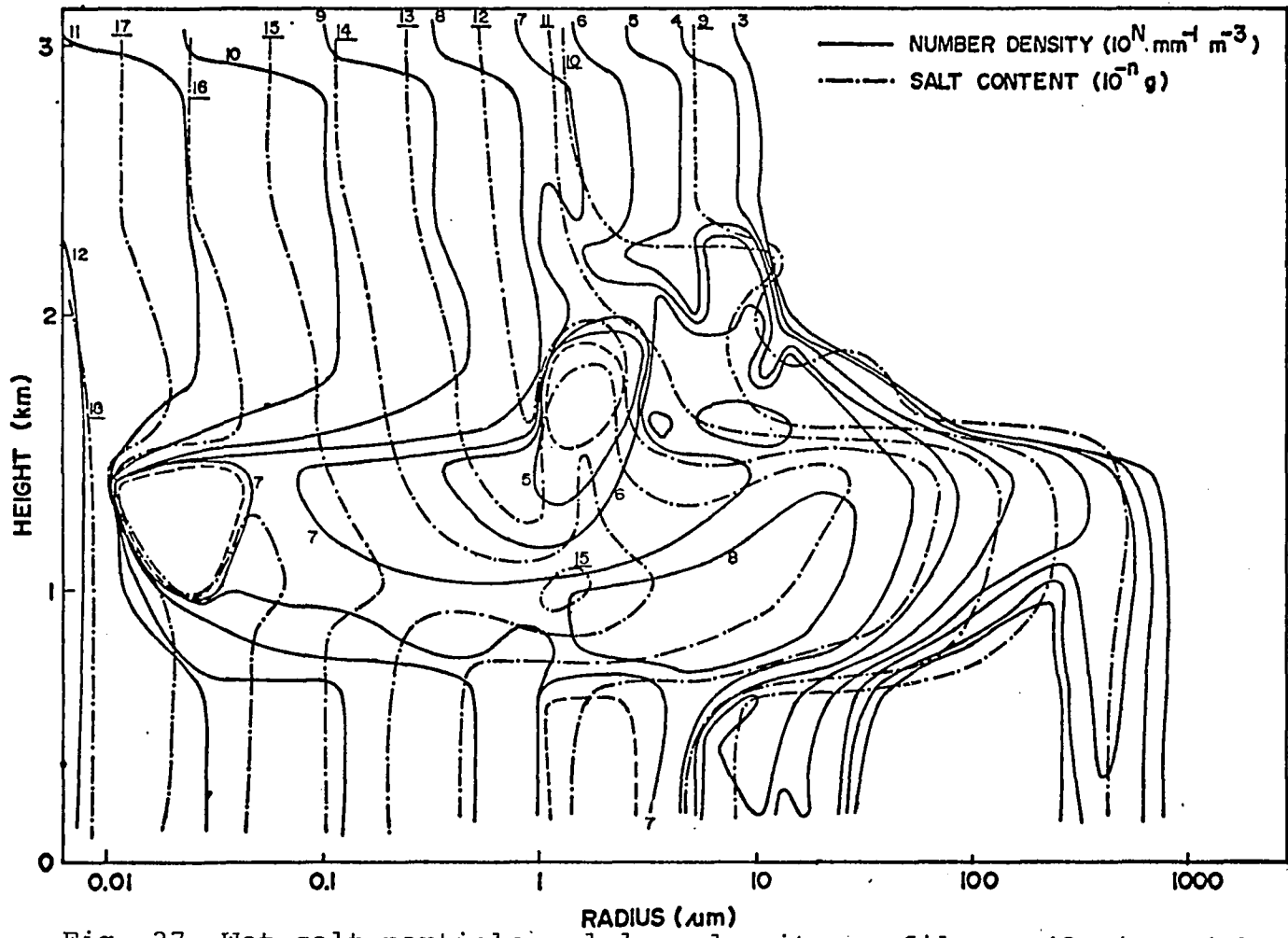


Fig. 27 Wet salt particle and drop density profile at 42 min, with the standard nucleus concentration divided by ten. Numbers associated with solid lines show N; underlined numbers show n.

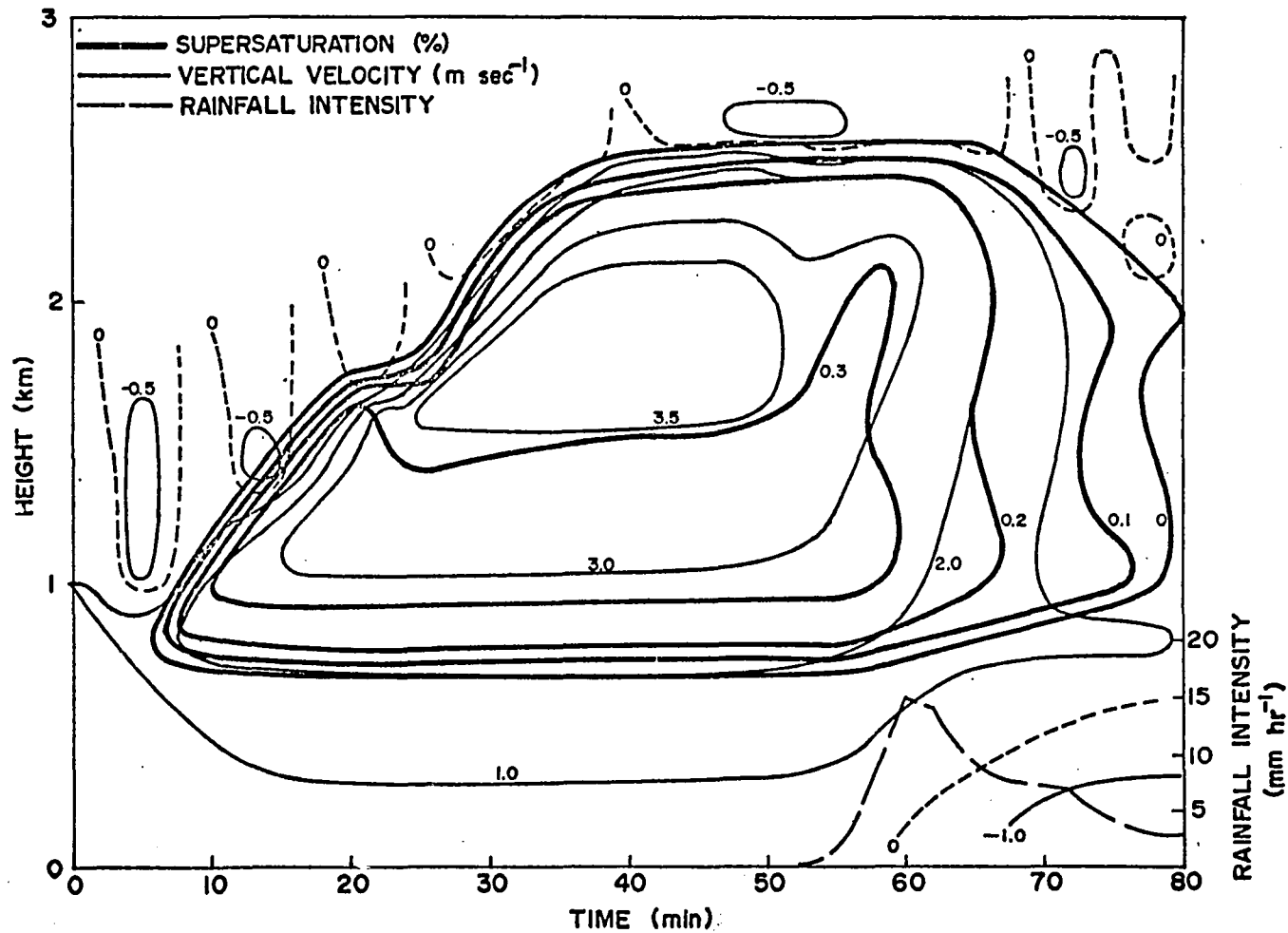


Fig. 28. Time-height variation of vertical velocity and supersaturation for the case of the standard nucleus concentration multiplied by ten.

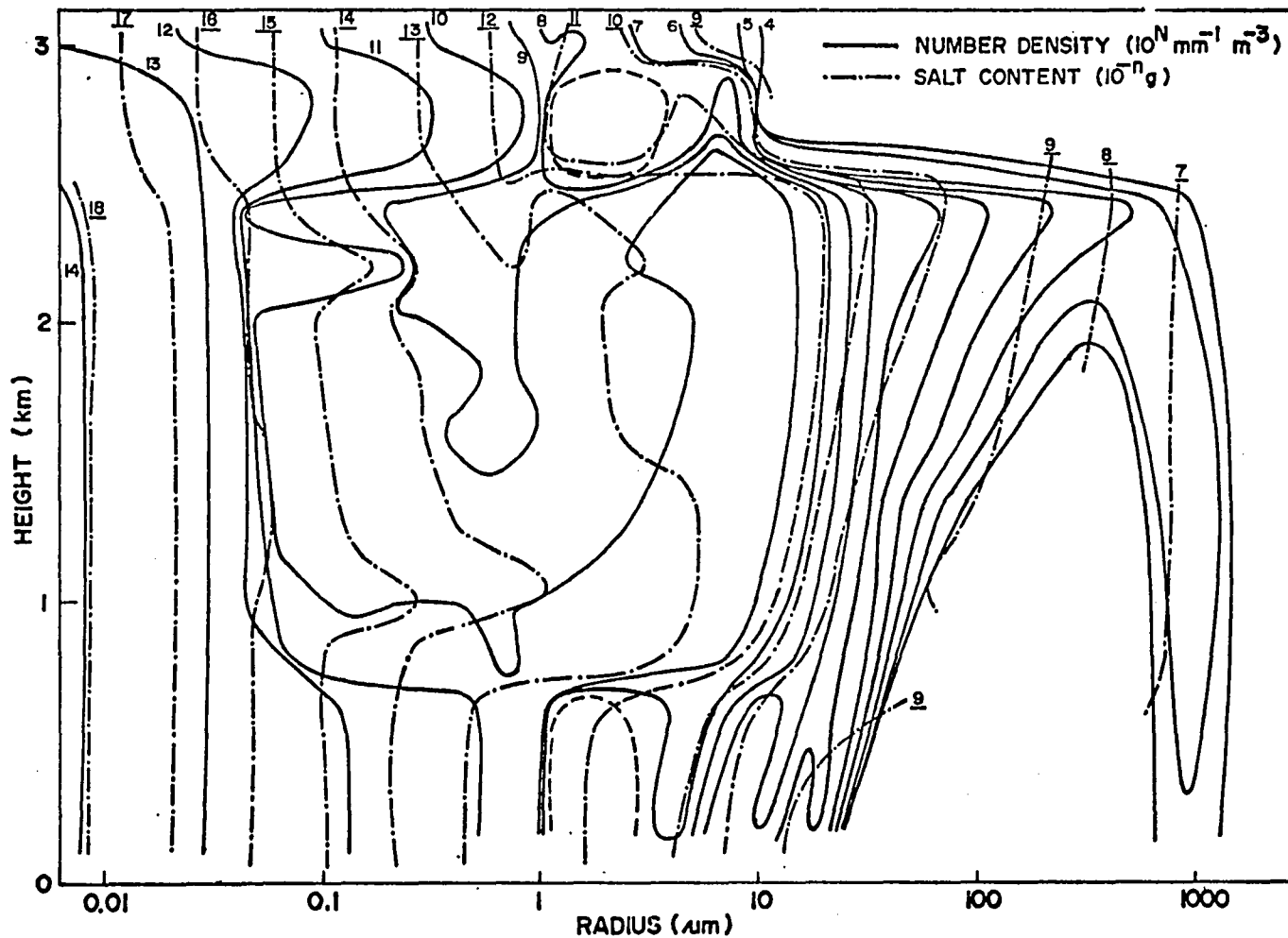


Fig. 29 Wet salt particle and drop density profiles at 56 min, with the standard nucleus concentration multiplied by ten. Numbers associated with solid lines show N ; underlined numbers show n .

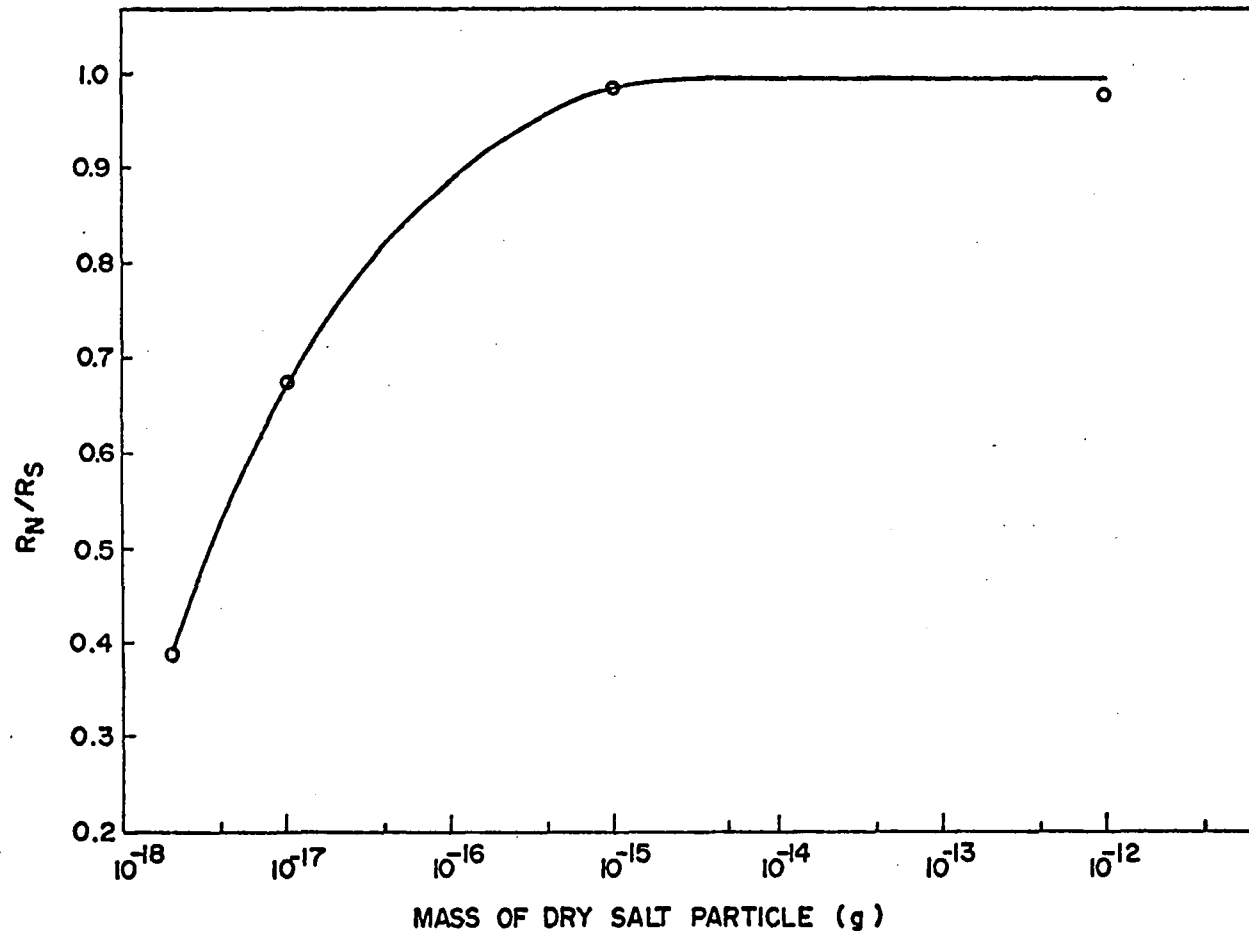


Fig. 30 Ratio of total rainfall amount with different nucleus size ranges (R_N) to that for the case with the standard nucleus distribution (R_S).

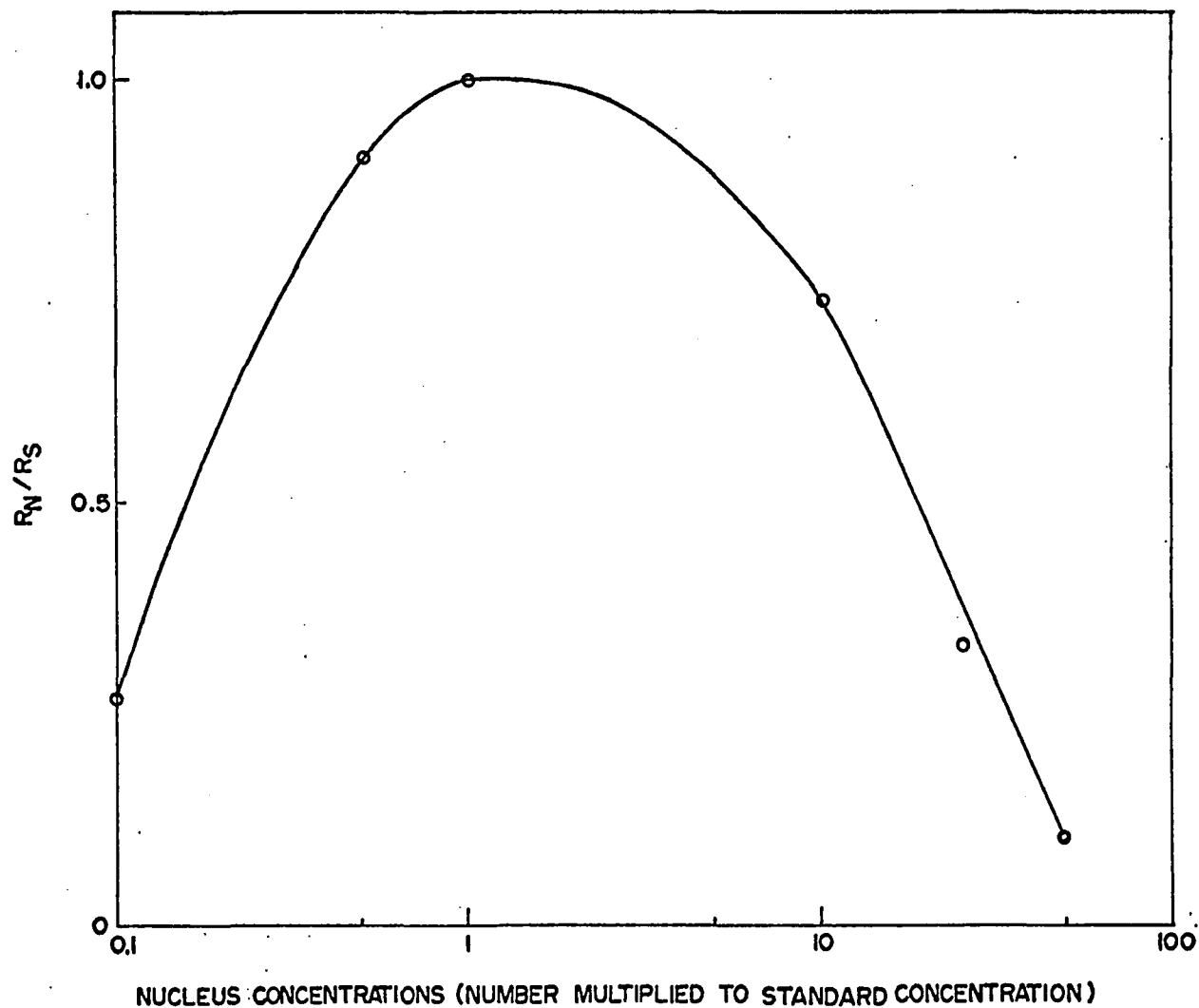


Fig. 31 Ratio of total rainfall amount with different nucleus concentrations (R_N) to that for the case with the standard nucleus distribution (R_S).

APPENDIX

List of Symbols

A	relative humidity in equilibrium at the surface of a drop.
A'	defined by Eq. (29)
A_0	constant defined by $2c_0/NoVob$
A_1, A_2, A_3	constants in Eq. (31)
A'_1, A'_2	constants in Eq. (32)
A''_1, A''_2, A''_3	constants in Eq. (33)
a	radius of cloud
a'	defined by $-B/\sigma$
B	defined by $3.2 \times 10^{-5}/T$
B'	defined by Eq. (30)
B_I	mobility of particles
b	constant collision kernel
C	defined by $8.6 m'_I/W$
C_α	defined by $1.7 \times 10^{-5} \alpha^{-1}$
C_β	defined by $1.5 \times 10^{-5} \alpha^{-1}$
C'	defined by C/σ
c_0	constant mass growth rate of condensation
c_p	specific heat of air at constant pressure
D	diffusion coefficient of water vapor in air
D_0	defined by Eq. (53)
D_a	diffusion coefficient of particles

D_f	defined by Eq. (23)
DJ	scale factor
E, E', E''	constants in Eqs. (31), (32) and (33)
F, F', F''	constants in Eqs. (31), (32) and (33)
F_L	drop number per unit volume in the size class L
$f(v, t)$	drop number density function
f_I	wet salt particle number per unit volume in the size class I
f_t	defined by Eq. (12)
$f_{3\alpha}$	correction term for the heat transfer at the surface of a drop
$f_{3\beta}$	correction term for the vapor transfer at the surface of a drop
f_{IK}^*	defined by Eq. (22)
G, G', G''	constants in Eqs. (31), (32) and (33)
G_O	defined by Eq. (54)
G_I, G_L	ventilation coefficients for particle and drop
g	acceleration due to gravity
$g[\ln r]$	drop mass density function on $\ln r$
H	relative humidity
H_a	thermal conductivity of salt
H_O	defined by Eq. (51)
K	thermal conductivity of air
k	Boltzmann's constant
L_α	defined by Eq. (17)
L_C	defined by Eq. (18)

L_V	latent heat of condensation
M_L	salt content of drops in the size class L
M_w	molecular weight of water
m	mass of dry salt particle
M_I	salt content of wet salt particles in the size class I
m'_I	mean salt content of a wet salt particle of radius r_I
N	dry salt particle concentration
N_0	initial drop concentration
P	atmospheric pressure
p	defined by $-a^{2/3}$
Q	defined by Eq. (28)
Q_V	water vapor mixing ratio
Q_w	liquid water mixing ratio
q	defined by $2(a/3) + C$
R	universal gas constant
Re_I, Re_L	Reynolds numbers for particle and drop
$RO(K)$	radius representing the smaller edge of particle size class K
$RT(K)$	radius after 2 sec growth by condensation starting from radius $RO(K)$
r	particle radius
r_I	particle radius in size class I
r_L	drop radius in size class L
r_0	radius of the smallest drop considered
S_{ca}	Schmidt number

S	variable used in Laplace transformation
T	temperature
T_V	virtual temperature
t	time
Δt	time step
t_{IK}	time required for a particle of radius r_I to grow to r_K
U	radial velocity
u	mass of a drop colliding with v-drop
v	mass of a drop
V_B	mean velocity of particles due to Brownian motion
V_D	mean velocity of particles due to diffusiophoresis
$V(L L')$	collection kernel of L-drop with respect to L' -drop
V_L, V'_L	terminal velocity of L-drop and L' -drop
V_T	mean velocity of particle due to thermophoresis
v_O	initial mean mass of drops
W	molecular weight of salt
w	vertical velocity
Δw	initial vertical velocity at $Z = 1$ km
X_L	mass of drops in the size class L
X_{LC}	defined by $X_L - X'_L$
x	defined by v/v_O
X_I	mass of particles in the size class I
$Y_C(L L')$	collision efficiency of L-drop with respect to L' -drop

y	defined by $r + \frac{a'}{3}$
y'	defined by u/v_0
Y_1, Y_2, Y_3	roots of Eq. (27)
z	height
z_0	constant height (1 km)
α	accommodation coefficient
α_0	mixing coefficient
β	condensation coefficient
Γ_d	adiabatic lapse rate
$\Delta, \Delta', \Delta''$	constants in Eqs. (31), (32) and (33)
δ	defined by Eq. (34)
ζ	defined by λ/r_I
η	dynamic viscosity of air
λ	mean free path of the air molecule
ξ	defined by $x - y'$
ρ	density of air
$\rho_{s\infty}$	saturation vapor density
σ	supersaturation
σ_c	critical supersaturation
τ	variable characterizing the fraction of N removed by collection at time t
$\Phi(s, \tau)$	Laplace transformation of $\Psi(x, \tau)$ defined by Eq. (45)
$\Psi(x, \tau)$	drop number density function defined by Eq. (37)

LITERATURE CITED

- Almeida, F. C., 1977: Collision efficiency, collision angle and impact velocity of hydrodynamically interacting cloud drops: A numerical study. J. Atmos. Sci., 34, 1286-1292.
- Arnason, G., and R. S. Greenfield, 1972: Micro- and macro-structure of numerically simulated convective clouds. J. Atmos. Sci., 29, 342-367.
- Asai, T., 1965: A numerical study of the air-mass transformation over the Japan Sea in winter. J. Meteor. Soc. Japan, 43, 1-15.
- Asai, T., and A. Kasahara, 1967: A theoretical study of the compensating downward motions associated with cumulus clouds. J. Atmos. Sci., 24, 487-496.
- Berry, E. X., 1967: Cloud droplet growth by collection. J. Atmos. Sci., 24, 688-701.
- Bowen, E. G., 1950: The formation of rain by coalescence. Aust. J. Sci. Res., A3, 193-213.
- Brown, E. N., and R. R. Braham, Jr., 1959: Precipitation particle measurements in trade-wind cumuli. J. Meteor., 16, 609-616.
- Clark, T. L., 1973: Numerical modeling of the dynamics and microphysics of warm cumulus convection. J. Atmos. Sci., 30, 857-878.
- Davies, C. N., 1966: Deposition from moving aerosols. Aerosol Science (Davies, C. N., ed.), New York, Academic Press, 393-440.
- Findeisen, W., 1939: Zur Frage der Regentropfenbildung in reinen Wasserwolken (On the question of raindrop formation in pure water clouds). Met. Z. 56, 365-368.
- Fitzgerald, J. W., 1974: Effect of aerosol composition on cloud droplet size distribution: A numerical study. J. Atmos. Sci., 31, 1358-1367.
- Fukuta, N., and L. A. Walter, 1970: Kinetics of hydrometeor growth from a vapor-spherical model. J. Atmos. Sci., 27, 1160-1172.

- Golovin, A. M., 1963: The solution of the coagulation equation for cloud droplets in a rising air current. Bull. Acad. Sci. USSR, Geophys. Ser., No. 5, 783-791.
- Gunn, R., and G. D. Kinzer, 1949: The terminal velocity of fall for water droplets in stagnant air. J. Meteor., 6, 243-248.
- Howell, W. E., 1949: The growth of cloud drops in uniformly cooled air. J. Meteor., 6, 134-149.
- Jiusto, J. E., 1967: Aerosol and cloud microphysics measurements in Hawaii. Tellus, 19, 359-368.
- Komabayasi, M., and K. Isono, 1967: Electric conductivity of rain water in the cloud over the island of Hawaii. Tellus, 16, 408-419.
- Korn, G. A., and T. M. Korn, 1961: Mathematical Handbook for Scientists and Engineers. New York, McGraw-Hill Book Company, 943 pp.
- Kovetz, A., and B. Olund, 1969: The effect of coalescence and condensation on rain formation in cloud of finite vertical extent. J. Atmos. Sci., 26, 1060-1065.
- Langmuir, I., 1948: The production of rain by chain reaction in cumulus clouds at temperatures above freezing. J. Meteor., 5, 175-192.
- Ludlam, F. H., 1951: The production of showers by the coalescence of cloud droplets. Quart. J. Roy. Meteor. Soc., 77, 402-417.
- Mason, B. J., and R. Emig, 1961: Calculations of the ascent of a saturated buoyant parcel with mixing. Quart. J. Roy. Meteor. Soc., 87, 212-222.
- Mason, B. J., and C. W. Chien, 1962: Cloud-droplet growth by condensation in cumulus. Quart. J. Roy. Meteor. Soc., 88, 136-142.
- Mason, B. J., 1971: The Physics of Clouds. Oxford, Clarendon Press, 613 pp.
- Mordy, W. A., 1959: Computations of growth by condensation of a population of cloud droplets. Tellus, 11, 16-44.

- Neiburger, M. and C. W. Chien, 1960: Computations of the growth of cloud droplets by condensation using an electronic digital computer. Physics of Precipitation, Geophys. Monogr. No. 5, Washington, D. C., Amer. Geophys. Union, 191-209.
- Nelson, L. D., 1971: A numerical study on the initiation of warm rain. J. Atmos. Sci., 28, 752-762.
- Ogura, Y. and T. Takahashi, 1973: The development of warm rain in a cumulus model. J. Atmos. Sci., 30, 262-277.
- Riehl, H., 1954: Tropical Meteorology. New York, McGraw-Hill Book Company, Inc., 392 pp.
- Scott, W. T., 1968: Analytic studies of cloud droplet coalescence I. J. Atmos. Sci., 25, 54-65.
- Shafir, O., and M. Neiburger, 1963: Collision efficiencies of two spheres falling in a viscous medium. J. Geophys. Res., 68, 4141-4148.
- Silverman, B. A., and M. Glass, 1973: A numerical simulation of warm cumulus clouds: Part I. Parameterized vs. non-parameterized microphysics. J. Atmos. Sci., 30, 1620-1637.
- Slinn, W. G. N., and J. M. Hales, 1971: A reevaluation of the role of thermophoresis as a mechanism in - and below - cloud scavenging. J. Atmos. Sci., 28, 1465-1471.
- Squires, P., and J. Warner, 1957: Some measurements in the orographic cloud of the island of Hawaii and in trade wind cumuli. Tellus, 9, 475-494.
- _____, 1958: The microstructure and colloidal stability of warm clouds. I. The relation between structure and stability. Tellus, 10, 256-261.
- Soong, S. T., 1974: Numerical simulation of warm rain development in an axi-symmetric cloud model. J. Atmos. Sci., 31, 1262-1285.
- Takahashi, T., 1973: Numerical simulation of maritime warm cumulus. J. Geophys. Res., 20, 6233-6247.

- Takahashi, T., 1975: Tropical showers in an axi-symmetric cloud model. J. Atmos. Sci., 32, 1318-1330.
- _____, 1976a: Warm rain, giant nuclei and chemical balance - A numerical model. J. Atmos. Sci., 33, 269-286.
- _____, 1976b: Rainfall at Hilo, Hawaii. J. Meteor. Soc. Japan, 55, 121-129.
- _____, 1977: A study of Hawaiian warm rain showers based on aircraft observation. J. Atmos. Sci., 34, 1773-1790.
- Telford, J., 1955: A new aspect of coalescence theory. J. Meteor., 12, 436-444.
- Turner, J. S., 1955: The salinity of rainfall as a function of drop size. Quart. J. Roy. Meteor. Soc., 81, 418-429.
- Twomey, S., 1959: The nuclei of natural cloud formation. Part II. The supersaturation in natural clouds and the variation of cloud droplet concentration. Geofis. Pura Appl., 43, 243-249.
- _____, 1966: Computations of rain formation by coalescence. J. Atmos. Sci., 23, 405-411.
- Waldmann, L., and K.H. Schmitt, 1966: Thermophoresis and diffusiophoresis of aerosols. Aerosol Science (Davies, C. N., ed.), New York, Academic Press, 137-161.
- Warner, J., 1955: The water content of cumuliform cloud. Tellus, 4, 449-457.
- _____, 1970: The microstructure of cumulus cloud. Part III. The nature of the updraft. J. Atmos. Sci., 27, 682-688.
- Warshaw, M., 1967: Cloud droplet coalescence: Statistical foundations and a one-dimensional sedimentation model. J. Atmos. Sci., 24, 278-286.
- _____, 1968: Cloud droplet coalescence: Effects of the Davis-Sartor collision efficiency. J. Atmos. Sci., 25, 874-877.

- Woodcock, A. H., 1950: Condensation nuclei and precipitation. J. Meteor., 7, 161-162.
- _____, 1951: Atmospheric salt particles and raindrops. J. Meteor., 9, 200-212.
- _____, 1972: Smaller salt particles in oceanic air and bubble behavior in the sea. J. Geophys. Res., 77, 5316-5321.
- _____, R. A. Duce and J. L. Moyers, 1971: Salt particles and raindrops in Hawaii. J. Atmos. Sci., 28, 1252-1257.
- Zebel, G., 1966: Coagulation of aerosols. Aerosol Science (Davies, C. N., ed.), New York, Academic Press, 31-57.